

Developments of Infrared Thermography-based Tools to Assist Surgical Procedures and Workflow

Dissertation
zur Erlangung des akademischen Grades
Dr. rer. med.

an der Medizinischen Fakultät
der Universität Leipzig

eingereicht von Michael Unger, M.Sc.

Geburtsdatum, Geburtsort: 09.11.1983, Köthen (Anhalt)

angefertigt an der Universität Leipzig, Innovation Center Computer Assisted
Surgery (ICCAS)

Betreuer: Prof. Dr. Thomas Neumuth

Beschluss über die Verleihung des Doktorgrades vom: 24.01.2023

Contents

1	Introduction	1
1.1	Thermography	3
1.1.1	Infrared thermal cameras	5
1.1.2	Benefits and limitations for medical applications	6
1.1.3	Medical applications of thermography	7
1.2	Workflow Assistance	9
2	Original Articles	13
2.1	Automatic detection of perforator vessels using infrared thermography in reconstructive surgery	13
2.2	Vision-based online recognition of surgical activities	23
2.3	Automatic depth scanning system for 3D infrared thermography	31
3	Summary	35
3.1	Conclusions and Outlook	39
4	References	40

1 Introduction

Temperature measurement is a daily routine in medicine to either be used for diagnosis or to monitor the course of a disease. Classical means to measure the body temperature include thermometers which provide knowledge of the general body temperature. When more insight into the temperature and its distribution over the body parts is needed, more advanced measurement techniques are necessary. Infrared thermography describes the process of imaging an object's surface temperature by detecting the electromagnetic radiation emitted by an object in the infrared spectrum. Thermal cameras, which are relatively common these days, were first used in the 1960s. The early models provided only a very limited number of imaging elements (<10) and had a low temperature and spatial resolution of 0.5 K and 5 mm, respectively [RA12]. The scanning rates of up to 16 images per second were lower compared to modern systems as well although not as limited as the other properties. Additionally, the detectors needed active cooling using e.g. nitrogen making these systems bulky and difficult to move and use. These factors limited the applicability for medical uses but enabled the first investigations on how the temperature of body parts is affected by diseases. Over the years, the temperature and spatial resolution improved leading to thermal cameras with 2048×1536 pixel resolution and thermal sensitivity of less than 10 mK. The devices became smaller resulting in very compact and lightweight cameras and improved scanning times of up to 120 images per second to enable dynamic temperature analysis.

The technological advancements of thermal cameras improved the overall usability making thermal cameras a vastly used imaging technique for medical applications [Lah12]. Thermography has been used to reveal pathologies or to monitor the treatment, but the analysis of the temperature measurements was mainly performed manually by the investigator. Tools assisting the application of thermography in clinical settings are lacking. Hence, the field of research in this work investigated technological improvements in thermography and previously uncovered applications for use in surgical environments.

The high sensitivity of thermal cameras enables the detection of very small temperature differences like these caused by blood vessels. In the literature, infrared thermography was used to detect blood vessels of microvascular tissue in reconstructive surgery. Infrared thermography was used to visually locate the perforator vessels of the deep inferior epigastric perforator (DIEP) flap by qualitative assessment of the skin temperature distribution [dWWM12a]. However, the results of this manual approach are impacted by the skill of the examining clinician as reading and interpreting thermographic images requires training. The perforator vessels cause a local temperature maximum as shown by de Weerd, but the temperature differences between a local minimum and a local maximum are quite small (~ 0.5 K) which leads to a low contrast image.

The objective of this work was the development and evaluation of a system that is capable of detecting local temperature maxima by analyzing the variations of the skin temperature to automatically identify the positions of the perforators in the thermogram and, therefore, make this method more reliable (article 1, section 2.1).

Imaging temperature can also be used to distinguish between live and inanimate objects which enables new applications for technical support systems in the operating room (OR). Operating rooms represent the most complex and expensive units of hospitals because a high percentage of hospital admissions is due to surgical interventions [GG11]. Providing technical assistance for complex manual tasks has the potential to increase the efficiency and efficacy of clinical processes. Ideally, assistance needs to be provided without interfering with the established treatment processes [SvdH06]. Hereby, the term workflow assistance was established which is explained here briefly and more detailed in section 1.2. Workflow assistance describes the process of automating manually performed tasks that can be tedious and repetitive for the staff. In a surgical context, manual tasks include, for example, setting up and configuring devices according to the type of intervention or even specifically for each patient. Thus, the team spends a reasonable amount of time on secondary tasks instead of the actual procedure. Workflow assistance provides a means to mitigate these effects. To provide workflow assistance, information on the ongoing processes is needed. State-of-the-art approaches to recognize surgical activities utilize visual cameras or additional sensors, but thermography hasn't been investigated for the recognition of surgical activities. The objective of this work was the development and evaluation of a system for the recognition of low-level tasks by analyzing thermal instead of visual data to simplify the extraction of regions of interest (article 2, section 2.2).

During the performed investigations, the limited depth of field of thermal cameras which is only in the range of some millimeters became evident. Additionally, due to the properties of the spectral range, typical thermal cameras don't provide automatic focus as known from visual cameras (see section 1.1.2). Some models providing an autofocus feature are available, but these models rely on range measurement and are intended for technical temperature measurements. The manual focusing is cumbersome and limits usability, especially during intraoperative use because sterility needs to be maintained. Furthermore, out-of-focus images negatively impact the accuracy of the temperature measurements due to the effects of blurring. This resulted in the objective to develop a thermographic system that acquires thermal images at varying focal planes and combines the measurements to reconstruct an all-in-focus image to improve the surface temperature measurement. This system enables a correct measurement of temperatures over a wide range of focal depths which can subsequently be used for image analysis (article 3, section 2.3).

Structure of the work

Section 1.1 gives a brief introduction to thermography including the foundations, technical limitations, and medical applications. An introduction to workflow assistance as well as why and how thermography can improve workflow assistance is given in section 1.2. The articles are included in section 2. Section 3 summarizes and discusses the articles included in this work and gives a brief outlook.

1.1 Thermography

Thermography describes the imaging process of an object's surface temperature. Thermographic cameras are able to detect electromagnetic radiation in the long-infrared range ($8\text{ }\mu\text{m} \dots 14\text{ }\mu\text{m}$).

Every object having a temperature above absolute zero (0 K; $-273.15\text{ }^{\circ}\text{C}$) is emitting electromagnetic radiation proportional to its temperature. Figure 1 shows the dependency of the spectral radiance with the wavelength for objects of different temperatures (Planck's law). With increasing temperature, the peak radiance shifts to a shorter wavelength. By integrating over the whole spectrum, the emitted radiation can be obtained according to the Stefan Boltzmann law. It states that the total emitted radiation M of a black body is directly proportional to the fourth power of the black body's temperature T :

$$M = \sigma * T^4 \tag{1}$$

A black body is an idealized physical object which absorbs all electromagnetic radiation, hence it is neither reflective nor transmissive. Therefore, this object emits the maximum possible radiation. Natural objects are described as gray bodies that emit far less radiation than a black body at the same temperature. The properties of a gray body can be described by the relation between the actual emitted radiation and that of a black body, called emissivity. Other properties are reflectivity, which describes how much radiation is reflected from the surroundings, and transmissivity, describing how radiation is passing through the object. The sum of emissivity ϵ , reflection ρ , and transmissivity τ is constant and equals one:

$$\epsilon + \rho + \tau = 1 \tag{2}$$

Because most materials do not show transmissivity in the infrared spectrum, the following applies:

$$\epsilon + \rho = 1 \tag{3}$$

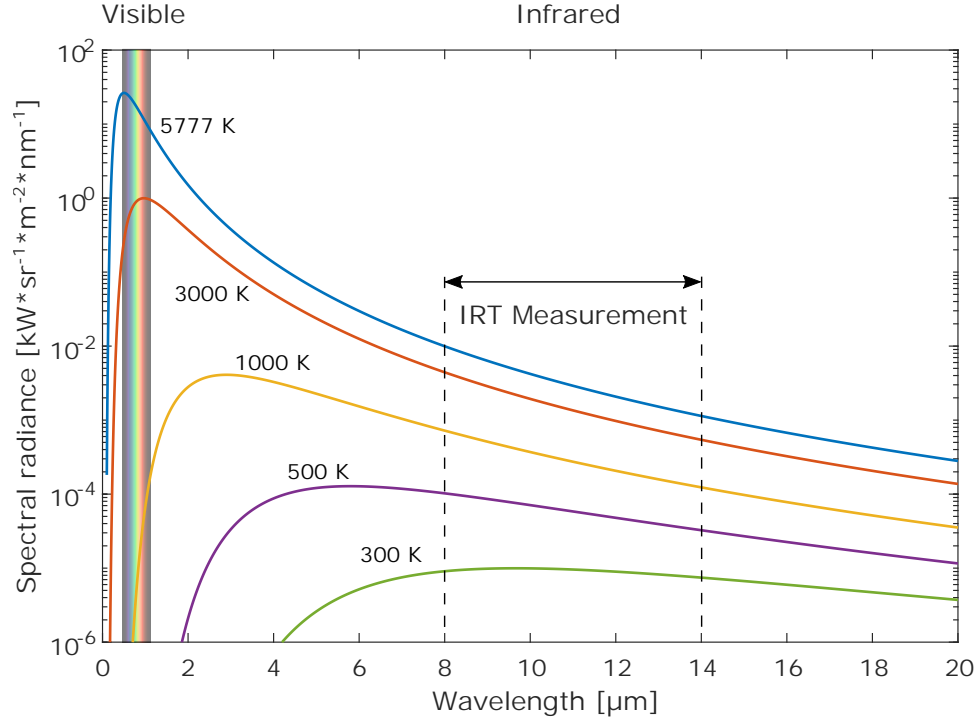


Figure 1: Planck's law describing the black-body radiation. The wavelength emitted radiation depends on the temperature of the object. Common thermal cameras measure the emitted radiation between 8 μm .. 14 μm to calculate the object's temperature.

The detected radiation of an object is the sum of the emitted and reflected radiation, and therefore impacts the temperature measurement. For example, surgical instruments made of metal have a low emissivity and a high reflectivity yielding wrong temperature measurements highly impacted by the temperature of the environment (Figure 2).

The object temperature can be calculated from the detected radiation using the Stefan Boltzmann law. The signal of the detector U is as follows:

$$U \sim \epsilon * T_{obj}^4 \quad (4)$$

As stated above, the reflected ambient temperature T_{amb} , as well as the temperature of the device T_{dev} , impacts the measurement, the formula changes as follows:

$$U \sim \epsilon * T_{obj}^4 + (1 - \epsilon) * T_{amb}^4 - T_{dev}^4 \quad (5)$$

The measured object temperature depends on its emissivity and the captured reflected ambient radiation. The emissivity is different for each material and may vary by temperature

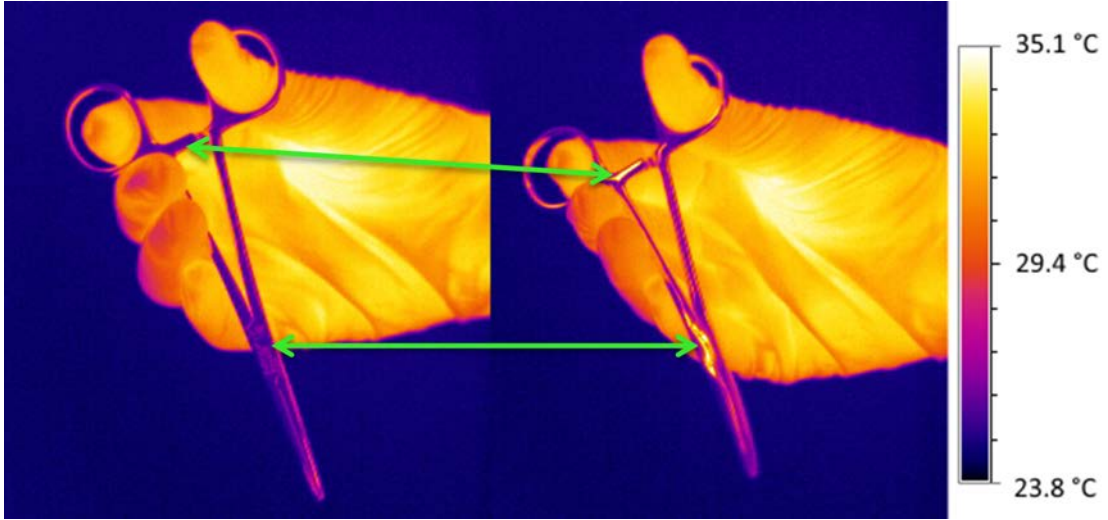


Figure 2: Surgical instrument made of steel. The reflectivity of the material results in false temperature measurements. The object reflects the radiation of the environment which results in inaccurate temperature measurement. On the left mostly the background was reflected, whereas on the right some warm object was reflected (indicated by the green arrows).

and wavelength. Deviance of the emissivity directly impacts the accuracy of the absolute temperature measurement, e.g. estimating the body core temperature by measuring the forehead temperature as used in fever thermometers. Steketee showed that the spectral emissivity of the skin is independent of the wavelength and equal to 0.98 ± 0.01 [Ste73]. Togawa investigated the emissivity of the skin for the forehead, forearm, palm, and back of the hand, and showed that the emissivity of the skin is independent of the region and equal to 0.971 ± 0.005 [Tog89]. Because this work is focused on temperature measurements of various body parts and only temperature differences are analyzed, the impact of different emissivities is omitted.

1.1.1 Infrared thermal cameras

Infrared detectors convert the absorbed electromagnetic radiation into an electrical signal proportional to the temperature of the object. The majority of optical detectors can be classified into two broad categories: photon detectors (also called quantum detectors) and thermal detectors [Rog12]. Photon detectors absorb the radiation, and the photo effect causes the electrons inside the semiconductor material to go into a higher energy level. When the electrons fall back to their natural energy level, an electrical signal is generated. Photon detectors exhibit a very fast response and good signal-to-noise ratio. To achieve this, the detectors must be cryogenically cooled to prevent the thermal generation of charge carriers, also known as Johnson-Nyquist noise, or thermal noise. Thermal detectors also absorb the incoming radiation. But in contrast

to photon detectors, the absorbed radiation changes the temperature of the detector material resulting in the change of physical properties to generate an electrical signal. Three approaches using different physical properties have been mainly used. Thermopiles (radiation thermocouples) generate a voltage, pyroelectric detectors change their electrical charge, and bolometers change their electrical resistance proportional to the temperature. Thermal detectors don't need to be cooled although cooled versions exist to increase the performance of the temperature measurement. Due to advancements in semiconductor technology in the last decades, thermal cameras using bolometers are most common for mobile devices. The imaging sensor consists of a focal plane array (FPA) of microbolometers and read-out circuitry. More detailed information on the different types of detectors and operation principles can be found in [Kru01; SJC58].

Currently, microbolometer-based thermal cameras provide spatial resolutions of up to 1024 x 768 pixels and thermal sensitivities of about 0.03 K. These thermal cameras can acquire images as fast as 80 frames per second making them suitable even for highly dynamic applications. The accuracy of the absolute temperature measurement mainly depends on the calibration effort. Commonly, vendors provide cameras with an accuracy of about 1 °C.

As stated above, the temperature measurement is impacted by the temperature of the device. When using an uncooled device its temperature will change over time caused by the self-heating of the electronic components. Therefore, a self-calibration is performed to compensate for the temperature drift over time. During this time (~ 1 s), temperature measurement isn't possible. After the self-calibration process, the temperature of the measured objects may leap depending on the temperature drift. This behavior needs to be considered and accounted for when measuring and analyzing the temperature over time. To mitigate these effects, the thermal camera needs to be in a thermally steady state. For measurements in the OR, this can be achieved by turning on the device well before measurement (at least 30 minutes) and by avoiding changing environmental conditions, e.g. moving the camera in and out of the laminar flow in the OR.

1.1.2 Benefits and limitations for medical applications

Thermal imaging is a contactless, passive and non-invasive imaging technique. The tissue doesn't need to be stimulated using external light or heat sources and no contrast agent needs to be administered. Therefore, thermal imaging doesn't need to deal with side effects. The property of being a contactless method provides advantages when used intraoperatively, where the sterility of instruments and devices is one of the main priorities. Modern thermal cameras provide real-time image acquisition enabling processing and analyzing temperature information over time. The high sensitivity makes thermal cameras suitable for the analysis of even the smallest temperature differences (< 100 mK).

The use of thermal cameras is limited when an accurate absolute temperature measurement is needed, especially when using uncooled devices. The accuracy of $1\text{ }^{\circ}\text{C}$ could be improved by placing an object of known temperature into the field of view and using this information as a reference for the recalibration of the device. This approach is very cumbersome, especially in an intraoperative setting. Endoscopic temperature measurement using thermal cameras is currently not available. Since thermal detectors operate in the long infrared range ($8\text{ }\mu\text{m}$ to $17\text{ }\mu\text{m}$) special materials are required to focus and guide the radiation through the endoscope to the imaging unit. Devices with the sensor located at the tip are possible, but the pixels of a microbolometer array are quite large ($\sim 17\text{ }\mu\text{m} \times 17\text{ }\mu\text{m}$) due to physical constraints compared to visual imaging sensors ($\sim 1.4\text{ }\mu\text{m} \times 1.4\text{ }\mu\text{m}$).

These large imaging sensors combined with a fixed large aperture result in a small depth of field (DOF), especially at small distances between camera and object. The DOF describes the distance between the farthest object and the nearest object that are acceptably sharp [SSZ09]. In the case of thermal cameras, blurred objects lead to a loss of information which results in incorrect temperature measurement and impacts the quality of subsequent image analysis. Various methods are available to acquire sharp images. The focusing solutions of classical RGB cameras are not applicable because thermal images might not show sharp edges, especially when depicting tissue. As the focus depends on the distance between camera and object, devices measuring the distance to an object via laser are available. This auto-focusing method improves the ease of use but objects out of the focal plane are still blurred. As the depth of field increases with the distance to the object, one solution is to measure the object at a greater distance. In return, this decreases the resolution of the pixels and might therefore not be applicable. Algorithms to extend the DOF exist but are highly dependent on the parameters of the image pre-processing [Sol12].

1.1.3 Medical applications of thermography

The human body is homeothermic and thus is generating heat and regulating the body's core temperature to stay stable at close to $37\text{ }^{\circ}\text{C}$. Whereas the body core temperature is relatively stable, the surface tissue, i.e. skin, forms part of the thermo-regulatory process. Changes in metabolic activity lead to changes in the surface temperature either locally or globally. Therefore, thermal imaging has been subject to numerous clinical studies investigating medical applications to reveal a possible pathology [Lah12]. For example, infrared thermography was used in medical applications for monitoring the skin temperature [Cha15], to detect a change in blood flow due to a clinical abnormality [RA12], skin cancer [HP11], inflammation [Den10; Pol17] and vascular disorders [Bag09; LEP17].

Physicians used the signs of inflammatory arthritis, like stiffness, pain, swelling, and heat, for diagnosis. The temperature increase of acutely inflamed joints is high enough to be easily detected by palpation. However, changes in temperature over time can be subtle depending on the course of the disease. Thermography can be used to objectively measure even the smallest temperature changes to assess the efficacy of treatment. Thermography was already used in the 1970s to objectively assess the duration and degree of reduction in inflammation during medication-assisted treatment [BRB79; Ess78]. Recently, Spalding et al. used thermal imaging to analyze the temperature distribution of arthritic joints and calculate a heat distribution index to create a quantifiable measure corresponding to changes in symptoms and physical exam findings [Spa08].

Infrared thermal imaging has been widely investigated for use in breast cancer screening [Ger14; Omr16; Vre13]. Malignant tumors are causing a localized increase in temperature which is visualized as spots or vascular patterns in breast infrared thermograms [Tan08]. Commercially available thermal cameras provided an increased thermal and spatial resolution over the last decades and the methodology of processing and analyzing the thermograms got more complex [Ger16]. Nonetheless, reports of low sensitivity and specificity conclude that there is currently insufficient evidence to recommend the use of these technologies for breast cancer screening [Vre13]. For the identification of brain tumors, studies revealed tumoral hypothermia in gliomas [Fio18; Nay17] which is expected to be caused by the decreased metabolism and lower density in tumor microvessels [Gor04].

Intraoperative imaging techniques enable an early analysis of the operation outcome. For example, indocyanine green (ICG) angiography is widely used to assess the reperfusion after anastomosis. Infrared thermography has been investigated for intra- and postoperative use to monitor microvascular free flaps following oropharyngeal reconstruction [Jus15]. Static and dynamic temperature analysis was used to assess the flap perfusion and detect perfusion failure. Infrared thermography has also been investigated for the evaluation of head tissue perfusion compared to ICG angiography during cranioplasty [Rat18]. A dynamic approach was chosen, by cold-challenging the investigated region of the skin and measuring the temperature over time. Parameters to assess the skin perfusion were defined for infrared thermography and compared to ICG perfusion parameters. A similarity between the parameters of both imaging techniques was shown.

In reconstructive surgery, the transfer of microvascular tissue is used to cover defects from tumor removal or malformations. A microvascular free flap usually consists of the skin, the subcutaneous layer, and muscle (Figure 3). The deep vessels branch into smaller vessels perforating the muscle and subcutaneous layer hence called perforator vessels. These further branch into a

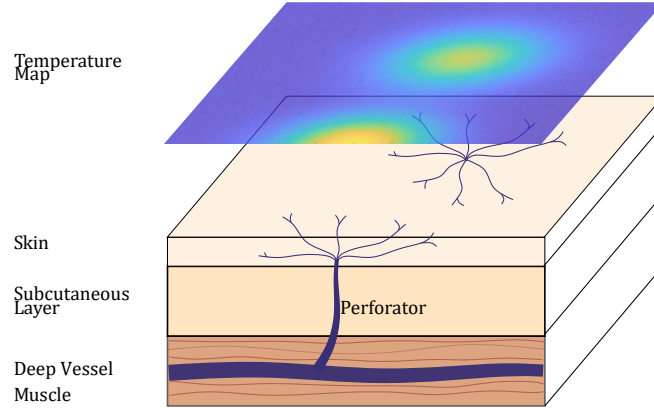


Figure 3: Representation of the anatomical skin model and the expected temperature distribution at the skin surface.

fine vessel system in the skin and can be made visible with thermal imaging, due to the blood's temperature being higher than its surrounding tissue. For a positive outcome of the procedure, the contour of the transplant must match the blood vessel network. Therefore, the location of the blood vessels supplying the transplant needs to be known during the planning of the skin harvesting. Hence, thermal imaging can be used to shorten pre-operative assessment and the detection of a matching donor area.

1.2 Workflow Assistance

Workflow assistance describes the process of automating manually performed tasks which can be used to relieve the surgical staff of tedious and repeating tasks. To automate tasks, the preceding, current, and predicted future situation in the OR needs to be known for reliable and intelligent system behavior [FMN15]. To enable this kind of behavior, the situation and activities in the OR need to be measured and matched to pre-existing workflow models. The course of surgical interventions can be described with surgical process models [Neu09]. This model represents only a specific procedure. A statistical mean of many models of the same intervention can be transformed into a generic surgical process model that describes one type of intervention [Neu11]. This model can be used to trigger automated tasks based on the progress of the intervention. The recognition of the progress in the OR is based on information acquired from the sources available in the OR. Information sources can be either medical devices, sensor data, or human input. Information from medical devices limits the assessment of the situation in the OR to device-related conditions, like the use of a microscope, endoscope, high-frequency devices, etc. Accessing information from medical devices is highly vendor-dependent and the

provided interfaces. Because this approach is quite limited in regards to which information can be obtained acquiring sensor data was more broadly investigated.

During a surgical procedure, the workflow is defined by tasks that are once or repeatedly executed in a specific order. One of the essential information is which task the surgeon is performing, as it provides direct knowledge of the progress of the procedure. Since many tasks involve manual instruments which don't provide information on their use or how it's being used per se, approaches on how additional sensors can be introduced to acquire the required information were investigated. The goal is the automatic identification of surgical instruments which closely relate to the tasks performed by the surgeon. Hand-held surgical instruments were outfitted with radio frequency identification (RFID) tags to detect instruments used in the situs [BJD09; Kra12; MN12; NM12; Van09]. RFID technology was also used to detect which instruments are used in laparoscopic surgeries for the recognition of surgical workflows [Miy09; Kra13].

To further get information on how the instrument is being used, inertial measurement units were attached to surgical instruments or the hands of the surgeon. This enables precise measuring and analyzing of the movements of the hands to classify the performed surgical task [Ahm08; Les05; NM12; Mei14]. The introduction of additional sensors simplifies the information acquisition from a technical point of view but requires the modification of instruments, which in turn impacts the commercial availability, and affects the usability and user experience. Hence, methods that don't require the modification of instruments are investigated.

Glaser et. al. proposed a multi-sensor table to detect instrument usage during a surgical procedure without the need to modify the instruments [GDN15]. Because almost all instruments are transferred to and from the table of the scrub nurse, it was modified with a digital scale and two cameras (visual and infrared) to automatically track instruments. This approach relied on visual information to recognize and track instruments. Because visual information is widely available, it provides a natural source of information about the situation in the OR. The surgical staff relies heavily on visual cues and, therefore, vision-based recognition is an obvious approach to acquire and process readily available information. Furthermore, vision-based approaches are also appealing because they are contact-less, cheap, and widely applicable.

In particular, vision-based human activity recognition has been an important area of research for many years as tasks and interactions in the OR are almost always human-related. Human activities can be categorized into four different levels with increasing complexity: gestures, actions, interactions, and group activities [AR11]. Gestures are the least complex and describe elementary movements of a person's body part that carry some meaning, like 'hand waving', or 'making an incision'. The combination of multiple gestures in a temporary order is called

an action, e.g. 'passing an instrument', or 'suturing'. Interactions are actions that involve two or more persons and/or objects, for example 'exchanging an instrument', or 'operating a device'. Group activities are the most complex activity and are performed by more than two persons and may involve objects, for example, 'the surgical team performing a procedure'. For the recognition of surgical tasks, the detection of low-level activities gestures and actions are most relevant. Therefore, the recognition of surgical instruments and the performed activities have been widely investigated. The video data of endoscopic and microscopic procedures were analyzed to determine low-level tasks [BFN10; Bou17; HZV12; Kla08; Lal13; Lal11].

In computer vision, the desired information can't be measured directly. Instead, the information provided by the sensor of the camera needs to be processed. The processing of information, called computer vision, includes major steps like segmentation, feature extraction and representation, and activity classification [BAH17]. Computer vision deals with challenges like changing brightness, occlusion, execution rate, background clutter, and camera motion which make each of the aforementioned steps more than trivial. Segmentation is a fundamental step in image processing to distinguish between the foreground and the background. The foreground contains regions of relevant information, like the person or surgical instrument. In contrast, the background contains no relevant information and needs to be filtered before applying image analysis. Hence, the correct segmentation of the image directly impacts the recognition performance. Image segmentation has been widely investigated and advanced over the years from simple region-based over model-based techniques to complex neural networks [Kha13]. The advances were founded on the various challenges that are encountered in computer vision. Due to changes in environmental conditions, the image of the same object may change over time. This might be caused by intentionally changing the brightness of the room lighting, shadowing due to occlusion of lights, or variation of daylight over time. Further difficulties arise from reflection which is often encountered in medical environments due to the usage of metallic instruments or light-colored devices. These various challenges caused the methods to become more and more complex to improve the robustness by covering all possible effects on the image.

Computer vision is widely focused on processing visual images. Extending the used information by expanding the spectral range to the non-visual infrared spectrum may further improve image processing and, therefore, the recognition of surgical tasks. Using the non-visible infrared spectrum enables contactless measurement of temperature, which is described in more detail in section 1.1. Knowledge of the temperature distribution within a scene enables distinguishing between live and inanimate objects. The region of interest for the recognition of gestures or actions can be more easily obtained by extracting the parts of the image which show an elevated temperature with respect to the background. Hence, the image segmentation process may be

further improved. Thermography has been used for human-computer interaction to recognize and classify hand gestures [App09] and for the recognition of facial expressions for people with severe motor impairments [MVC09]. But thermography hasn't been used for the recognition of surgical activities.

In conclusion, the recognition of low-level tasks is the first step of higher-level assistance systems based on workflow recognition. Although the information on the low-level tasks can be easily acquired via the introduction of additional sensors, the need to modify existing medical devices hampers the translation of this research. Methods that don't require additional sensors provide advantages in that respect. The recognition of low-level tasks via commonly used visual cameras is a complex topic, especially when dealing with changing environmental conditions. A novel approach of low-level task recognition based on methods of machine learning to analyze thermal instead of visual data was proposed which simplifies the extraction of regions of interest by analyzing alternative imaging modalities (see article: Development and evaluation of a method to recognize surgical tasks - section 2.2).

2 Original Articles

This work consists of the three original articles which are presented in the following sections:

- Unger M, Markfort M, Halama D, Chalopin C (2019) Automatic detection of perforator vessels using infrared thermography in reconstructive surgery. *Int J CARS* 14:501?507. <https://doi.org/10.1007/s11548-018-1892-6>
IF: 2.5 (2019)
- Unger M, Chalopin C, Neumuth T (2014) Vision-based online recognition of surgical activities. *Int J CARS* 9:979?986. <https://doi.org/10.1007/s11548-014-0994-z>
IF: 1.7 (2014)
- Unger M, Franke A, Chalopin C (2016) Automatic depth scanning system for 3D infrared thermography. *Current Directions in Biomedical Engineering* 2:369?372. <https://doi.org/10.1515/cdbme-2016-0162>
IF: 0.5 (2015)

Automatic detection of perforator vessels using infrared thermography in reconstructive surgery

Michael Unger, Miriam Markfort, Dirk Halama & Claire Chalopin

International Journal of Computer Assisted Radiology and Surgery

A journal for interdisciplinary research, development and applications of image guided diagnosis and therapy

ISSN 1861-6410

Int J CARS

DOI 10.1007/s11548-018-1892-6



Your article is protected by copyright and all rights are held exclusively by CARS. This e-offprint is for personal use only and shall not be self-archived in electronic repositories. If you wish to self-archive your article, please use the accepted manuscript version for posting on your own website. You may further deposit the accepted manuscript version in any repository, provided it is only made publicly available 12 months after official publication or later and provided acknowledgement is given to the original source of publication and a link is inserted to the published article on Springer's website. The link must be accompanied by the following text: "The final publication is available at link.springer.com".



Automatic detection of perforator vessels using infrared thermography in reconstructive surgery

Michael Unger¹ · Miriam Markfort² · Dirk Halama² · Claire Chalopin¹

Received: 17 May 2018 / Accepted: 28 November 2018
© CARS 2018

Abstract

Purpose Knowing the location of the blood vessels supplying the skin and subcutaneous tissue is a requirement during the planning of tissue transfer in reconstructive surgery. Commonly used imaging techniques such as computed tomography angiography and indocyanine green angiography expose the patient to radiation or a contrast agent, respectively. Infrared thermal imaging was evaluated with success as a non-invasive alternative. To support the interpretation of thermograms, a method to automatically detect the perforators was developed and evaluated.

Methods A system consisting of a thermal camera, a PC and custom software was developed. The temperature variations of the skin surface were analysed to extract the perforator locations. A study was conducted to assess the performance of the algorithm by comparing the detection results of the algorithm with manually labelled thermal images by two clinicians of the deep inferior epigastric perforator flap of 20 healthy volunteers.

Results The F measure, precision and recall were used to evaluate the system performance. The median F measure is 0.833, the median precision is 0.80, and the median recall is 0.907.

Conclusion The results of this study showed that it is possible to automatically and reliably detect the skin perforators in thermograms despite their weak temperature signature. Infrared thermal imaging is a non-invasive and contactless approach suitable for intraoperative use. Combined with a computer-assisted tool for the automatic detection of perforator vessels, it is a relevant alternative intraoperative imaging method to the standard indocyanine green angiography.

Keywords Non-invasive imaging · Automatic segmentation · Operation planning · Skin transplant

Introduction

Reconstructive surgery restores lost functionalities of body parts, for example, caused by injuries, tumour removal or malformations. Transfer of microvascular tissue has become a routine method for covering these defects [1]. These transplants, called flaps, include skin, subcutaneous tissue, and blood vessels. Main arteries and veins branch off into smaller blood vessels of diameter less than 1 mm which perforate subcutaneous tissue perpendicular to the skin surface. Hence, these vascular structures are called perforator vessels. After selection and extraction, the donor flap is transferred to the

damaged area and revascularised using microsurgery. Hence, knowledge of the anatomy of blood vessels is essential for an optimal flap selection.

The anatomy of blood vessels is individual for each patient. Therefore, several imaging techniques for the visualisation of perforator vessels exist. Digital subtraction angiography (DSA), computed tomography angiography (CTA) and magnetic resonance angiography (MRA) are used pre-operatively. They offer images of highest quality but require the administration of a contrast agent. Moreover, CTA and DSA expose the patient to radiation. Suitable perforators are still commonly annotated manually by a radiologist by interpreting the reconstructed imaging data [2,3], although computer-aided tools for the semi-automatic segmentation and report generation are emerging [4,5].

Furthermore, the flap selection will be made during the intervention in the operating room (OR), because the flap size depends on the actual defect [6]. Hence, additional intraoperative imaging techniques are required. Doppler ultrasound

Michael Unger
michael.unger@iccas.de

¹ Innovation Center Computer Assisted Surgery, University Leipzig, Semmelweisstr. 14, 04103 Leipzig, Germany

² Department of Oral, Maxillofacial and Plastic Facial Surgery, University Hospital Leipzig, Leipzig, Germany

(Doppler-US) and indocyanine green angiography (ICG-A) are commonly used. Doppler-US is a non-invasive technique for locating blood vessels, but its quality depends on device settings and the skill of the surgeon [7]. Furthermore, Doppler-US is prone to false positives, because even small vessels unsuitable for supplying the transplant are detected [8]. ICG-A is currently the standard procedure for intraoperative imaging. ICG is a fluorescent dye which is administered intravenously. The perforator vessels and its branching vessels are made visible with an infrared camera by exciting the dye using a light source. Because of the half-life of the dye of 3–4 min, repeated imaging is only possible after approximately 20 min. Although the incident rates of ICG are very low, it is not a risk-free procedure [9].

Infrared thermography (IRT) is a contactless imaging technique used to visualise the surface temperature of objects. Because physiological processes have an impact on the tissue temperature, thermography is widely used in medical applications to reveal a possible pathology [10]. For example, IRT was used in medical applications for monitoring the skin temperature [11], to detect skin cancer [12], breast tumours [13–15], inflammation [16,17] and vascular disorders [18,19].

The vascular system transports energy in the form of heat from the inner body to the surface. Thus, thermography can be used to detect perforator vessels in the skin. De Weerd used infrared thermography to visually locate perforator vessels by qualitative assessment of thermograms of the deep inferior epigastric perforator (DIEP) flap [20]. However, reading and interpreting thermographic images require training. Therefore, the quality of the analysis depends on the experience of the clinician conducting the examination. The perforator positions are detectable as local temperature maxima. However, the temperature differences at the skin surface are low and thus lead to low contrast in the thermogram. A tool to automatically identify the positions of the perforators in the thermogram would make this method more reliable.

Therefore in this paper, we propose an algorithm to locate perforator vessels of a free flap automatically. The output of the algorithm was compared to manually labelled images of two clinicians for the DIEP flap.

Material and methods

System design

An imaging system consisting of a thermal camera PI 450 (Optris GmbH, Berlin, Germany), a computer and custom-developed software was developed. The prototypical system is depicted in Fig. 1. The thermal camera is connected to the computer via USB and provides a spatial resolution of 382×288 pixels. The thermal sensitivity (NETD) of the cam-

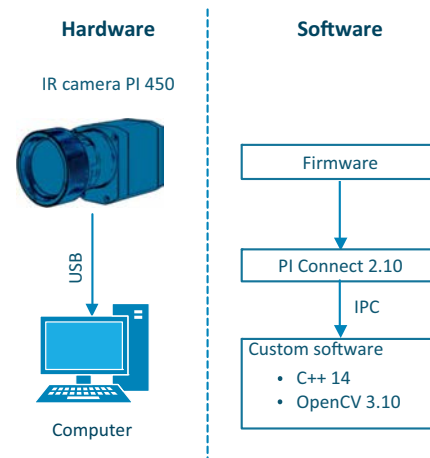


Fig. 1 Overview of the system components

era is 40 mK. By using optics with a field of view (FOV) of $13^\circ \times 10^\circ$, the pixel size (IFOV) is 0.6 mm at a given distance of 1 m between camera and object, and the measurement area is approximately $234 \text{ mm} \times 175 \text{ mm}$.

The thermal camera comes with imaging software (PI Connect version 2.10) which handles the device communication and image acquisition. Radiation emitted by objects is captured by the camera. Via a calibration done by the manufacturer, these radiation values are converted into temperature values.

To correctly measure the temperature of an object, its emissivity needs to be known. The emissivity describes how much energy is emitted as thermal radiation at a given object temperature. If the emissivity is not set correctly, the measured temperature values differ from the real object temperature. Steketee [21] showed that the emissivity of skin tissue is nearly constant. Therefore, a constant emissivity of 0.98 was used. Although the emissivity depends on the angle between object and camera [22], Schmidt et al. showed that the temperature error induced by the viewing angle could be neglected for angles up to 45° to the surface normal [23].

Perforator detection algorithm

Figure 2 shows the image processing steps to detect and visualise the perforators.

Data acquisition

The thermal camera only provides information about the energy emitted by the object in its field of view. The conversion of these radiometric data into temperature information

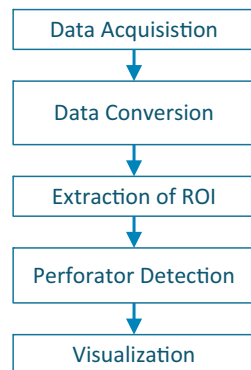


Fig. 2 Image processing steps for the automatic detection of perforator locations

is done by the vendor software PI connect. To retrieve the temperature values, our custom software is communicating with the vendor software using a dynamic link library (DLL).

Data conversion

Because some of the used computer vision functions require 8-bit greyscale images, the image is saved in that format. As a consequence of this, the temperature range needs to be reduced to preserve the thermal resolution. Thus, the temperature data are stored in an 8-bit greyscale image covering a temperature range of 25.8–38 °C at a thermal resolution of 50 mK.

Extraction of the region of interest (ROI)

The ROI describes the area which contains the perforators of the donor flap. The clinician defines the ROI by applying markers to the skin, which are visible in the visual image as well as in the thermal image. Surgical strips coated with metallic ink were used to provide visual cues in both image modalities while specifying the ROI.

Perforator detection

A perforator can be described by its centre and the supplied region of the skin. De Weerd et al. [20] showed that perforators correspond to hot spots in the thermal image. Hence, finding the perforator locations corresponds to finding the local temperature maxima in an image.

The image is preprocessed by applying a Gaussian blur filter to reduce noise. The kernel size (aperture size) of this filter has an impact on the perforator detection. A small value may lead to false positives because of noise induced by the imaging sensor, whereas a large value prevents the detection



Fig. 3 System set-up in the OR. The volunteer laid on the OR table. The thermal camera was directed at the DIEP flap. A laptop computer was used for the image acquisition

of small perforator vessels. Therefore, choosing an optimal value determines the detection result of the algorithm by suppressing false positives while being sensitive enough to detect small perforators.

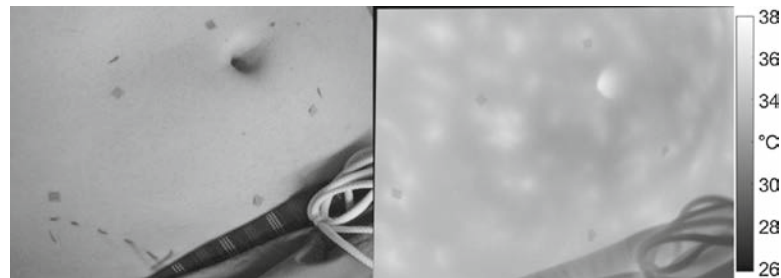
A local maximum is defined as one or more adjacent pixels having a higher value than their neighbours. To find the local maxima, the intensity values of the image are sorted. A breadth-first search approach was used to iterate over the pixels sorted by intensities. Beginning with the highest value, the pixel and its neighbours of the same value are labelled as a possible candidate for a local maximum. If no neighbours (8 connectivity) having higher intensity exists, then the pixels belong to a regional maximum. If a neighbour has a higher value, it is part of another hot spot.

In conclusion, the kernel size of the Gaussian filter is the unique parameter of the algorithm. Its value will influence the number of detected perforator centres.

Study design

An evaluation study, which was approved by the ethics committee, was conducted under intraoperative conditions at the Leipzig University Hospital. The participants were positioned on the operating table (see Fig. 3). The laminar flow of the OR's air conditioning was used to induce slight excitation of the skin temperature and enhance the contrast in the thermogram. This procedure was proposed by de Weerd et al. as a mild cold challenge [20].

Fig. 4 The visual image of the abdomen (left) and the corresponding thermal image (right). Dark colours correspond to cold temperatures, whereas bright colours correspond to warm temperatures. Markings on the skin denote the pelvic bone as an anatomical landmark



The deep inferior epigastric perforator (DIEP) is one of the most commonly used free flaps in reconstructive surgery. Therefore, the algorithm was evaluated using this region. As an example, Fig. 4 shows the temperature distribution as well as the corresponding visual image.

Five markers arranged in a convex polygon were used to define the ROI. Pixels outside this area were set to black to be ignored by the detection algorithm as well as during the manual labelling by the clinician.

Labelling of perforators

The acquired images were labelled by clinicians to evaluate the algorithm performance. Two clinicians, one experienced in reconstructive surgery and one medical student, labelled the perforator centres inside the ROI for each image. Figure 5c shows an example for the labelled perforators.

A tool for the annotation of the image data was implemented with ImageJ. Because of the small temperature variances, the clinicians could adjust the brightness and contrast of each data set.

Result classification

For result classification, the perforator centres automatically provided by the algorithm were compared to the manual labelling performed by the clinicians. If the distance between the manually labelled perforator centre and the centre detected by the algorithm was less than 10 pixel (approximately 6 mm), the result was classified as true positive. Otherwise, the result was classified as false positive if a perforator centre was detected by the algorithm but was not manually labelled within this radius. Equivalently, the result was classified as false negative if a perforator centre was manually labelled but no centre detected by the algorithm was within this radius.

Manually labelled and automatically detected centres, which were closer to the border of the ROI than half of the kernel size, were ignored during classification because the actual temperature maximum might be located outside of the ROI.

Composition of participants

Twenty participants were included in this study, ten males and ten females. The mean age was 27, ranging from 21 to 45. The mean body mass index was 21.95, ranging from 18.14 to 25.95.

Six participants were smokers. The mean amount was 6.8 pack-years, ranging from 1.5 pack-years to 15 pack-years. Ten participants noted they were doing sports regularly.

Results

The algorithm performance was evaluated using the F measure, recall, and precision. Moreover, the algorithm was tested with varying values of the kernel size ranging from 9 to 31 pixel to assess its effect on the results (Fig. 6).

The algorithm performance and body mass index for each volunteer are shown in Fig. 7. No significant correlation between BMI and algorithm performance was measured.

Discussion

The automatic detection of perforator vessel can subsequently support the surgeon during reconstructive surgery. The visual identification of locations containing perforators in the thermograms requires a learning process. Moreover, depending on surrounding conditions, different physiological or anatomical conditions of the patients, the images show low contrast and are difficult to interpret. Therefore, analysing the temperature distribution in an area of interest and presenting the perforator location can support the surgeon during the flap selection. A study was conducted to evaluate the system performance by comparing the detection algorithm to perforator locations labelled by clinicians for different values of the kernel size of the Gaussian filter.

The F measure, which is defined as the harmonic mean of precision and recall, was used to evaluate the system performance. The best median score of 0.833 was reached for a

Fig. 5 Post-processing steps. Thermal image acquired by the camera (a). Extracted region of interest (b). Annotated perforators (c). Classification result (d). A green cross denotes the centre labelled by the clinician, and a red cross denotes the centre found by the algorithm. A green circle denotes true positive classification, a blue circle corresponds to a false negative classification, and a red circle denotes a false positive classification. The size of the circle shows the radius used for true positive classification. A plus denotes ignored recognition results due to close proximity to the ROI border

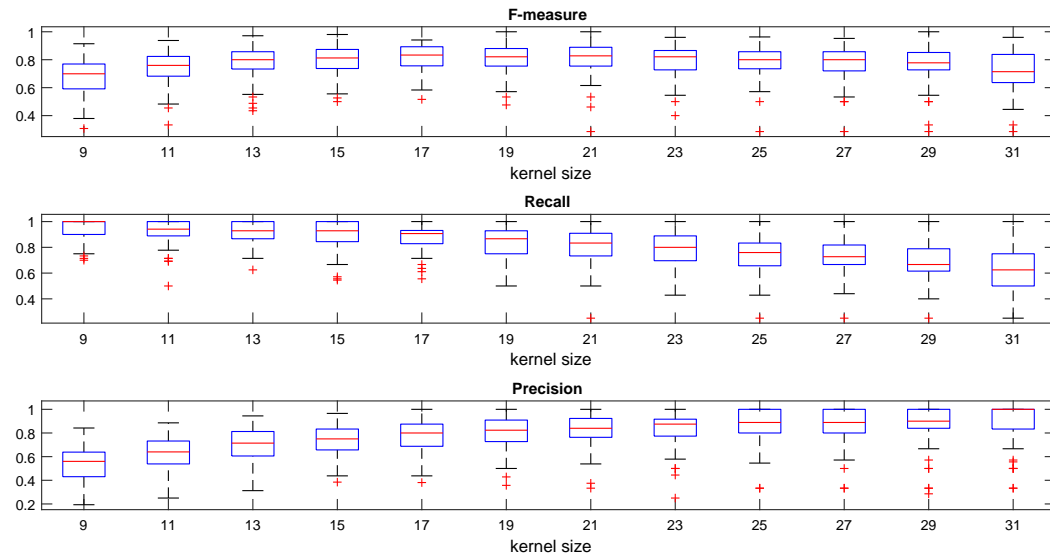
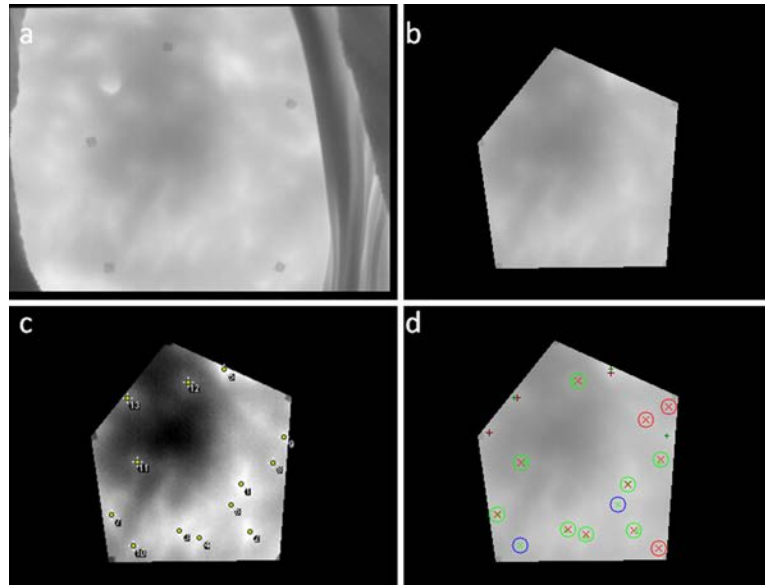


Fig. 6 Algorithm performance for the DIEP region of both clinicians. The best F measure (top) of 0.833 (median) is reached for a kernel size of 17. For this parameter value, the median recall is 0.907 (middle) and the median precision is 0.80 (bottom)

kernel size of 17. Smaller kernel sizes lead to the detection of more positives caused by the reduced filtering. Thus, the recall, which is defined as the proportion of correctly detected perforators over all perforators labelled by the clinicians, is higher for smaller kernel sizes at the cost of increased detec-

tion of false positives. In contrast, choosing a bigger kernel size leads to detecting fewer positives. Hence, the precision, which is defined as the proportion of correctly detected perforators over all perforators detected by the algorithm, is better for bigger kernel sizes. Therefore, the sensitivity of the sys-

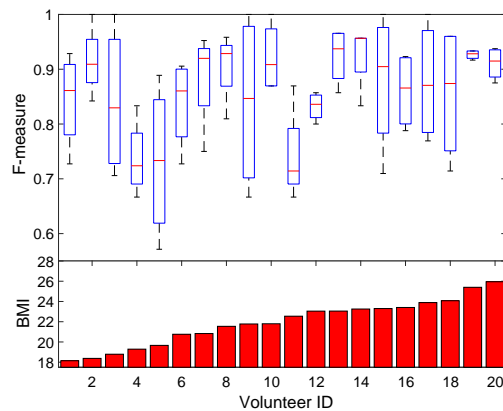


Fig. 7 Algorithm performance for each volunteer using a kernel size of 17 (top) sorted by body mass index (bottom). Each data set includes the left and right DIEP flap

tems can be adjusted by varying the kernel size. This enables the clinician to choose an optimal value depending on the specific patient and the region under examination. Although the algorithm performance varies, the current number of volunteers enrolled in the study, it is not enough to highlight statistically significant differences regarding specific parameters such as gender, age or daily sport activity. Currently, the algorithm was only evaluated for the region of the DIEP flap. More studies are needed to assess the performance of typical donor flap regions.

Furthermore, the algorithm was compared to images manually labelled by clinicians, which provides an initial indication whether a thermography-based system is suitable for the detection of perforator vessels. However, by using the manually labelled images as a gold standard, the results are affected by the skills and experience of the clinician. Hence, the system performance needs to be further evaluated by comparing the detection results of the algorithm with a second imaging technique. For example, CT angiography is used pre-operatively during reconstructive surgery and is therefore suitable for comparing the perforator locations detected by the algorithm with the actual position of the blood vessels.

At the current development stage, the algorithm facilitates the perforator identification because no manual adjustment of brightness and contrast is needed. In particular, images with low contrast are harder to interpret and manual analysis requires more time. The main goal in the intraoperative workflow is to find the main perforator(s). Perforators with low perfusion are not suitable as a donor and should be excluded. One approach could be the exclusion of detected perforators with a small temperature difference of less than e.g. 200 mK. The impact of the usability, user acceptance and impact on the clinical workflow must be investigated further.

Conclusion

A system consisting of a thermal camera and custom software was developed to detect perforator vessels. This approach is usable for pre- and intraoperative imaging. In contrast to CT and MR angiography as well as ICG angiography, it is a non-invasive technique. No contrast agent is necessary for imaging, and therefore the examination can be repeated as needed. This characteristic enables on-demand imaging in the operating room which might offer advantages in case of changing requirements for the donor flap due to changes in the tumour resection process.

Only static thermal images were analysed to detect the locations of the perforator vessels. Multiple static images can be combined to improve the recognition robustness over time. Dynamic thermograms are a promising approach in the early detection of breast cancer [24,25], and therefore might improve the perforator detection. By cooling the skin surface and analysing its reheating, the strength of underlying vessels can be estimated. A study investigating dynamic analysis needs to be conducted to assess the feasibility and performance of this approach.

Acknowledgements The project was funded by the German Federal Ministry of Education and Research (BMBF) in the scope of Zentrales Innovationsprogramm Mittelstand (ZIM) (Grant Number KF 2026723AK4).

Compliance with ethical standards

Conflict of interest The authors declare no conflict of interest.

Ethical approval All procedures performed in studies involving human participants were in accordance with the ethical standards of the institutional and/or national research committee and with the 1964 Declaration of Helsinki and its later amendments or comparable ethical standards.

Informed consent Informed consent was obtained from all individual participants included in the study.

References

- Gardiner MD, Nanchahal J (2010) Strategies to ensure success of microvascular free tissue transfer. *J Plast Reconstr Aesthet Surg* 63(9):e665–e673
- Wade RG, Watford J, Wormald JCR, Bramhall RJ, Figus A (2018) Perforator mapping reduces the operative time of DIEP flap breast reconstruction: a systematic review and meta-analysis of preoperative ultrasound, computed tomography and magnetic resonance angiography. *J Plast Reconstr Aesthet Surg* 71(4):468–477
- Cina A, Barone-Adesi L, Rinaldi P, Cipriani A, Salgarello M, Masetti R, Bonomo L (2013) Planning deep inferior epigastric perforator flaps for breast reconstruction: a comparison between multidetector computed tomography and magnetic resonance angiography. *Eur Radiol* 23(8):2333–2343

4. Lange CJ, Thimmappa ND, Boddu SR, Dutruel SP, Pei M, Farooq Z, Heshmatzadeh Behzadi A, Wang Y, Zabih R, Prince MR (2017) Automating perforator flap MRA and CTA reporting. *J Digit Imaging* 30(3):350–357
5. Chae MP, Hunter-Smith DJ, Rozen WM (2016) Comparative study of software techniques for 3d mapping of perforators in deep inferior epigastric artery perforator flap planning. *Gland Surg* 5(2):99–106
6. Wong C-H, Wei F-C (2010) Microsurgical free flap in head and neck reconstruction. *Head Neck* 32(9):1236–1245
7. Rozen WM, Phillips TJ, Ashton MW, Stella DL, Gibson RN, Taylor GI (2008) Preoperative imaging for DIEA perforator flaps: a comparative study of computed tomographic angiography and doppler ultrasound. *Plast Reconstr Surg* 121(1):9
8. Giunta R, Geisweid A, Feller AM (2000) The value of preoperative doppler sonography for planning free perforator flaps. *Plast Reconstr Surg* 105(7):2381–2386
9. Marshall MV, Rasmussen JC, Tan I-C, Aldrich MB, Adams KE, Wang X, Fife CE, Maus EA, Smith LA, Sevvick-Muraca EM (2010) Near-infrared fluorescence imaging in humans with indocyanine green: a review and update. *Open Surg Oncol J* 2(2):12–25
10. Lahiri BB, Bagavathiappan S, Jayakumar T, Philip J (2012) Medical applications of infrared thermography: a review. *Infrared Phys Technol* 55(4):221–235
11. Chang K, Yoon S, Sheth N, Seidel M, Antalek M, Ahad J, Darlington T, Ikeda A, Kato GJ, Ackerman H, Gorbach AM (2015) Rapid vs. delayed infrared responses after ischemia reveal recruitment of different vascular beds. *Quant Infrared Thermogr J* 12(2):173–183
12. Pirtini Çetingül M, Herman C (2011) Quantification of the thermal signature of a melanoma lesion. *Int J Therm Sci* 50(4):421–431
13. Vreugdenburg TD, Willis CD, Mundy L, Hiller JE (2013) A systematic review of elastography, electrical impedance scanning, and digital infrared thermography for breast cancer screening and diagnosis. *Breast Cancer Res Treat* 137(3):665–676
14. Gerasimova E, Audit B, Roux SG, Khalil A, Gileva O, Argoul F, Naimark O, Arneodo A (2014) Wavelet-based multifractal analysis of dynamic infrared thermograms to assist in early breast cancer diagnosis. *Front Physiol* 5:176
15. Omranipour R, Kazemian A, Alipour S, Najafi M, Alidoosti M, Navid M, Alikhassii A, Ahmadinejad N, Bagheri K, Izadi S (2016) Comparison of the accuracy of thermography and mammography in the detection of breast cancer. *Breast Care* 11(4):260–264
16. Denoble AE, Hall N, Pieper CF, Kraus VB (2010) Patellar skin surface temperature by thermography reflects knee osteoarthritis severity. *Clin Med Insights Arthritis Musculoskelet Disord* 3:69–75
17. Polidori G, Renard Y, Lorimier S, Pron H, Derruau S, Taiar R (2017) Medical infrared thermography assistance in the surgical treatment of axillary hidradenitis suppurativa: a case report. *Int J Surg Case Rep* 34:56–59
18. Bagavathiappan S, Saravanan T, Philip J, Jayakumar T, Raj B, Karunanithi R, Panicker TMR, Paul Korath M, Jagadeesan K (2009) Infrared thermal imaging for detection of peripheral vascular disorders. *J Med Phys* 34(1):43–47
19. Lin PH, Echeverria A, Poi MJ (2017) Infrared thermography in the diagnosis and management of vasculitis. *J Vasc Surg Cases Innov Tech* 3(3):112–114
20. de Weerd L, Weum S, Mercer JB (2012) Dynamic infrared thermography (DIRT) in the preoperative, intraoperative and post-operative phase of DIEP flap surgery. *J Plast Reconstr Aesthet Surg* 65(5):694–695
21. Steketee J (1973) Spectral emissivity of skin and pericardium. *Phys Med Biol* 18(5):686
22. Zimmermann T, Zimmermann M (2012) *Lehrbuch der Infrarotthermografie: allgemeine Grundlagen der Thermodynamik, Grundlagen der Strahlungsphysik, Infrarot-Geräte-Technologie (für normative Stufe 1 und 2)*. Fraunhofer IRB-Verl, Stuttgart. OCLC:816255129
23. Schmidt E, Eckert E (1935) Über die Richtungsverteilung der Wärmestrahlung von Oberflächen. *Forschung auf dem Gebiet des Ingenieurwesens A* 6(4):175–183
24. Gerasimova-Chechkina E, Toner B, Marin Z, Audit B, Roux SG, Argoul F, Khalil A, Gileva O, Naimark O, Arneodo A (2016) Comparative multifractal analysis of dynamic infrared thermograms and X-ray mammograms enlightens changes in the environment of malignant tumors. *Front Physiol* 7:336
25. Gerasimova-Chechkina E, Toner B, Marin Z, Audit B, Roux SG, Argoul F, Khalil A, Gileva O, Naimark O, Arneodo A (2016) Combining multifractal analyses of digital mammograms and infrared thermograms to assist in early breast cancer diagnosis. In: *AIP conference proceedings*, vol 1760. AIP Publishing, Melville, p 020018

Vision-based online recognition of surgical activities

Michael Unger · Claire Chalopin · Thomas Neumuth

Received: 11 December 2013 / Accepted: 7 March 2014 / Published online: 25 March 2014
 © CARS 2014

Abstract

Purpose Surgical processes are complex entities characterized by expressive models and data. Recognizable activities define each surgical process. The principal limitation of current vision-based recognition methods is inefficiency due to the large amount of information captured during a surgical procedure. To overcome this technical challenge, we introduce a surgical gesture recognition system using temperature-based recognition.

Methods An infrared thermal camera was combined with a hierarchical temporal memory and was used during surgical procedures. The recordings were analyzed for recognition of surgical activities. The image sequence information acquired included hand temperatures. This datum was analyzed to perform gesture extraction and recognition based on heat differences between the surgeon's warm hands and the colder background of the environment.

Results The system was validated by simulating a functional endoscopic sinus surgery, a common type of otolaryngologic surgery. The thermal camera was directed toward the hands of the surgeon while handling different instruments. The system achieved an online recognition accuracy of 96 % with high precision and recall rates of approximately 60 %.

Conclusion Vision-based recognition methods are the current best practice approaches for monitoring surgical processes. Problems of information overflow and extended recognition times in vision-based approaches were overcome by changing the spectral range to infrared. This change enables the real-time recognition of surgical activities and provides

online monitoring information to surgical assistance systems and workflow management systems.

Keywords Computer-assisted surgery · Workflow · Surgical process model · Intraoperative monitoring · Surgical activity recognition · Thermal imaging

Introduction

Modern operating rooms (ORs) are sophisticated technical systems that rely on various technologies and manifold processes [1, 2]. Complex medical devices are used to support surgical actions and to improve patient safety. However, the increasing use of technology also makes it necessary to interact with a variety of devices and to process the large amount of information provided by the surgical assistance systems. To design technical infrastructure in the OR to appropriately support the surgical team and to make improvements in healthcare processes, precise workflow models are required. This requirement drives the need to acquire information about the surgical processes themselves [3].

Surgical activities are complex processes that need models to describe them. In recent years, methods of modeling and analyzing processes have been developed [4, 5]. These methods are capable of describing surgical workflows, despite the high complexity and variation of surgical tasks.

A surgical intervention is usually structured in interventional phases. The phases denote sections within an operation that end with a certain goal. A phase consists of multiple sequences of surgical activities that are identified using sensor data. The identification of the surgical activities is an important step in modeling the workflow of the surgery. The applications are surgical workflow management sys-

M. Unger (✉) · C. Chalopin · T. Neumuth
 Innovation Center Computer Assisted Surgery, University of Leipzig,
 Semmelweisstr. 14, Leipzig 04103, Germany
 e-mail: michael.unger@medizin.uni-leipzig.de

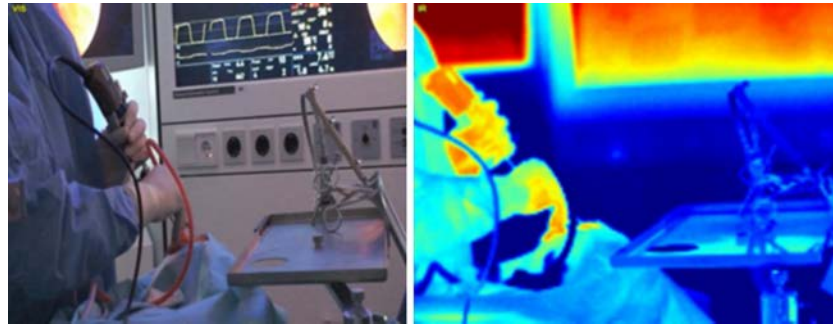


Fig. 1 Visual image and the corresponding thermal image (with *red color* denoting warm areas and *blue color* denoting cold areas)

tems that provide robust guidance for surgical activities [6]. These workflow management systems may trigger devices and automate the documentation of surgical procedures or the estimation of operation end times [7]. Furthermore, knowledge of ongoing interventional phases [8] and operation end times exceeding their estimated duration is needed in the field of anesthesia [10].

Several strategies exist to identify surgical activities. If surgical interventions are performed using robotic systems, mechanical tracking information can be used to acquire information about the movements of the robot without the need to alter the technical systems or instruments. Therefore, a surgical process can be analyzed based on these trajectories without biasing the process. It has been shown that motion data generated during robotic surgery can be used to recognize surgical activities and to evaluate the skills of a surgeon [11–13].

When no robotic systems are used in an intervention, additional sensors must be brought into the process. Radio frequency identification (RFID) is used to track the use of surgical instruments and the presence of personnel in the OR [14–18]. Using accelerometers, it is possible to recognize the activities performed by the surgeon [19,20]. Recognition of the use of surgical instruments using RFID is accurate but has the drawback of necessary modification of the instruments. If the surgeon has to wear accelerometers, this feature can lead to constraints in motion and affect the quality of the work.

To overcome this problem, vision-based approaches can be used to identify surgical processes based on video data [21–25]. It has been shown that methods based on video data performed equally well as approaches based on kinematic data.

The main limitation of vision-based methods for the automatic recognition of surgical activities in the surgical workflow is the extraction of objects of interest. Video images of the operating field include a large amount of information, such as information about the surgeon's hands, the surgical instruments, or the patient. The image quality and contrast

are not always optimal because of the specific lighting in the OR. The segmentation task, which has to be automatic due to the large dataset, is therefore complex.

The use of thermographic information acquired by infrared thermal cameras can overcome this problem. Furthermore, the temperature measurements provide unique information, in contrast to approaches using conventional visual images (see Fig. 1). We propose a system combining an infrared thermal camera with an object recognition system for the automatic online identification of surgical activities. We show that the use of thermal data has advantages over conventional video data and is suitable for the recognition of surgical activities. This article presents the approach needed to develop a system that is capable of recognizing surgical activities online.

System design

Activity recognition system overview

Thermography has been successfully used to recognize and classify hand gestures [26]. Information on hand temperatures enables easier extraction of gestures than in video images under good acquisition conditions. Our system consists of a thermal camera as the imaging modality and of software for surgical gesture recognition (see Fig. 2).

The camera acquires thermal images from the surgical scene. Subsequently, segmentation, object detection, and gesture recognition are performed. The segmentation removes the background from each image. The object detection provides information about the position of possible gestures. This information is used to extract sub-images of the original thermal image. These images are used by the gesture recognition algorithm to identify surgical activities.

The software was developed in C++. The OpenCV software library provided algorithms for processing the images from the thermal camera.

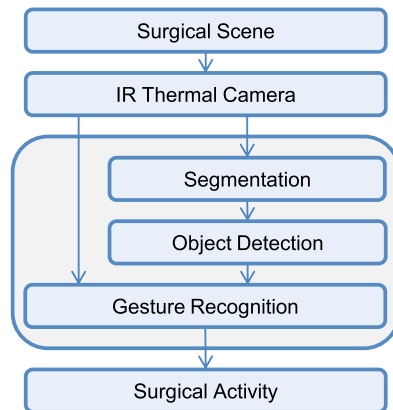


Fig. 2 Structure of the system

Thermal imaging modality

The infrared camera measures the thermal radiation emitted by the objects and bodies in a scene. The radiation data are converted into temperature values based on a calibration process. Software provided by the manufacturer handles the communication with the camera and provides the temperature data via an API.

We used the thermal camera PI160 from the company Optris¹ (see Fig. 3). The camera works on a spectral range of 8–14 μm . The thermal resolution or noise equivalent temperature difference (NETD) is 100 mK, and the resolution of the images is 160×120 pixels. Images are acquired at up to 120 frames per second. The accuracy is $\pm 2^\circ\text{C}$. The given parameters of the optics ($23^\circ \times 17^\circ$, 10 mm) and the distance of 1.5 m to the surgical scene yield a field of view of 0.60×0.44 m.

The acquired thermal images were retrieved from the camera software using a DLL that was provided by the system vendor.

Segmentation

A segmentation step was performed to remove the background and to segment the surgeon's hands as regions of interest. Figure 4 shows images acquired during a simulated surgery, and Fig. 5 depicts the segmentation results. The image was scaled to a range of 20–40 $^\circ\text{C}$. The colors are grayscale representations (values of 0 to 255) of the temperature of the pixels. Dark colors denote cold objects (here, the background, the patient, and the surgical instruments), whereas light colors denote warm objects (here, the surgeon and, more specifically, the surgeon's hands). The images were



Fig. 3 Thermal camera Optris PI160

thresholded using a temperature value of 32°C , keeping only the hands, with a surface temperature of $32\text{--}35^\circ\text{C}$, in the images.

Object detection

Next, the thresholded images were processed by a blob detection algorithm. The algorithm creates areas of connected components for the pixels masked by the thresholding. The given blobs are regarded as objects that will be classified. Small blobs are rejected to remove noise. In the study, we used a minimal pixel count of 80 to robustly detect the hands of the surgeon and to reject noised caused by other warm parts of the body. Using the position of the blobs, sub-images of 50×50 pixels, which included gestures, were extracted from the original thermal image (see Fig. 6).

Gesture recognition

We used hierarchical temporal memory (HTM) to classify the data. HTM was developed to model the structural and functional properties of the human neocortex [27, 28]. This model allows the classification of unknown images into categories by combining the principles of Bayesian networks and clustering algorithms. HTM has already been used to classify hand shapes under large variation in hand rotation [29]. Furthermore, another study [30] showed that it is possible to use HTM to recognize signed words. Both approaches are vision based.

HTM is hierarchically organized into multiple levels. Each level contains a certain number of so-called nodes. The lowest layer is connected to the sensor data. In our case, the sensor data are images showing a surgical gesture. Each node receives its input data from one or more nodes of a lower level and transmits its output data to a node of a higher level.

¹ <http://www.optris.com/>.

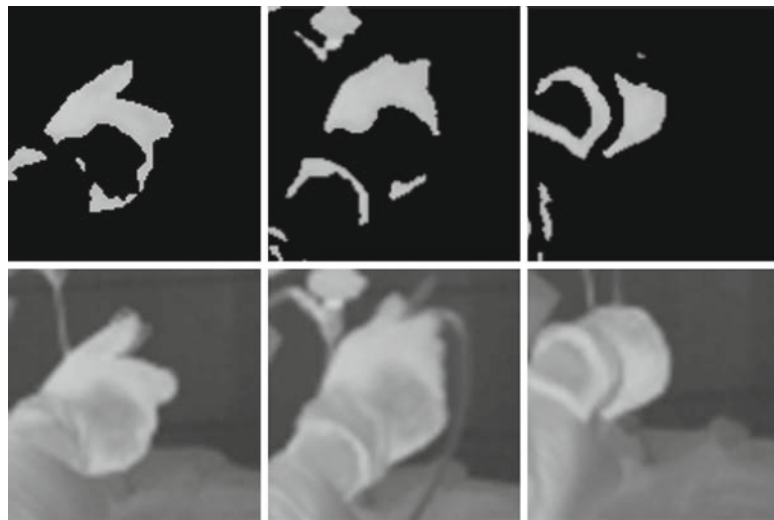
Fig. 4 Surgeon handling a blakesley (a), a suction tool (b), and an elevator (c)



Fig. 5 Segmentation of Fig. 4



Fig. 6 Extracted sub-images corresponding to the images in Fig. 5



Two different types of nodes exist: spatial and temporal nodes. In spatial nodes, reoccurring spatial patterns form coincidences, whereas temporal nodes recognize a correlation in sequences of spatial patterns. The coincidences are the output of nodes of lower order and the input of nodes of higher order. Thus, the details of an object are stored in the lower nodes, whereas the higher nodes recognize objects based on the composition of the objects' details.

The use of HTM requires two steps: a training phase and an inference phase. In the training phase, the network learns to recognize different categories based on images belonging to known categories that are provided by the user. Thus, each layer of the network needs to be trained successively. Beginning with the lower levels, each node is presented with input data and thus learns coincidences. The last step is the training of the classifier. Therefore, supervised learning is required to feed the classifier both input data and the corresponding cat-

egories. In our application, the categories represent different surgical gestures. In the inference phase, the network is able to classify an unknown image into a category.

We used the HTM implementation of NuPIC open-source software.² For the recognition of gestures, a seven-layer network was used. The first level was a thermal image of 50×50 pixels. A Gabor filter was used for edge detection in the input image. Two layers of spatial nodes and two layers of temporal nodes were used to recognize coincidences. Classification of the data was performed using the k-nearest neighbor algorithm (KNN). The KNN is a relatively simple classifier, and its disadvantage is that a high computational effort is needed when using large training sets. However, as mentioned before, recognition is performed in multiple layers. Thus, the KNN only needs to be trained to classify coin-

² <http://www.numenta.org/>.

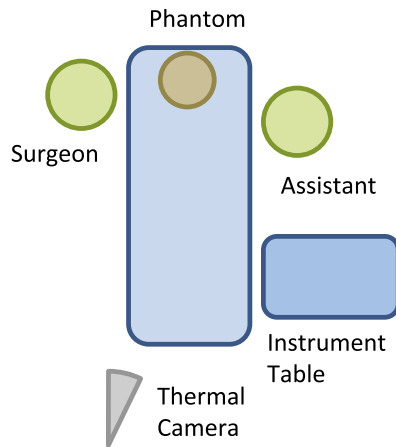


Fig. 7 Experimental setup of the simulated surgeries

cidences at the underlying level. Therefore, only a limited number of coincidences need to be trained. The amount of data is reduced, and therefore, the computational effort is moderate. The parameter $k = 1$ yielded optimal classification results for our data.

Evaluation study

Study design

Simulated clinical datasets

For system validation and accuracy estimation, a simulated functional endoscopic sinus surgery (FESS) was performed and recorded with a thermal camera. Students acting as the surgeon and an assistant performed the simulated surgery on a phantom.

The surgical scripts were based on the workflows of previously recorded real surgeries. The activities forming the intervention were announced to the actors by a recorded voice. Thus, a steady workflow was ensured throughout multiple passes. Three different workflows representing different operations were recorded four times each. Therefore, a total of 12 videos were recorded. The length of a single workflow was approximately 20 min, and all workflows contained 734 surgical activities. The study setup is shown in Fig. 7.

Recognition training and validation

During the surgical intervention, different activity types were performed by the surgeon. These activities were removal of tissue, movement of tissue, endoscopic imaging, documentation, cleaning of the endoscope, suction, injection of anes-

thetic, and disinfection. Additionally, a ninth category, *no gesture*, was introduced. The activities were classified as *no gesture* when the surgeon performed none of the eight surgical activities. For example, the handing of an instrument from the assistant to the surgeon and vice versa was classified as *no gesture*.

The videos were processed using a frame rate of two frames per second. The gold standard was defined by manual classification of each object recognized by the software. This step consists of the following procedure. The software is used to process the video data and to extract the gestures into sub-images. The sub-images are manually classified into one of the nine categories described above. The result is a dataset of gestures for each of the 12 videos, categorized into nine categories.

For validation, leave-one-out cross-validation was chosen. Gestures from 11 simulated operations were used to train the HTM network, whereas the gestures from the 12th simulated operation were classified. This procedure was repeated 12 times by changing the video of the operation used for classification each time. The output of the software was a vector of classified gestures that were compared with the previously defined gold standard.

Study results

During the processing of the 12 videos, a total of 60,199 gesture frames were classified. Binary classification was used to measure the performance of our system. We used accuracy, precision, and recall as measures. Accuracy denotes the true positives and true negatives among all gestures. Precision describes the true positives among all positives classified. Recall measures the true positives among all true gestures. The recognition results of our system are listed in Table 1. The column listing occurrence values gives an overview of how often a gesture occurred during the 12 interventions.

The results showed a high overall accuracy (between 89 and 99 %) and a low standard deviation (between 0 and 6 %). The precision values varied between 23 and 98 % and showed a standard deviation between 8 and 28 %. The recall rate ranged from 29 to 99 %, and the standard deviation was between 1 and 26 %.

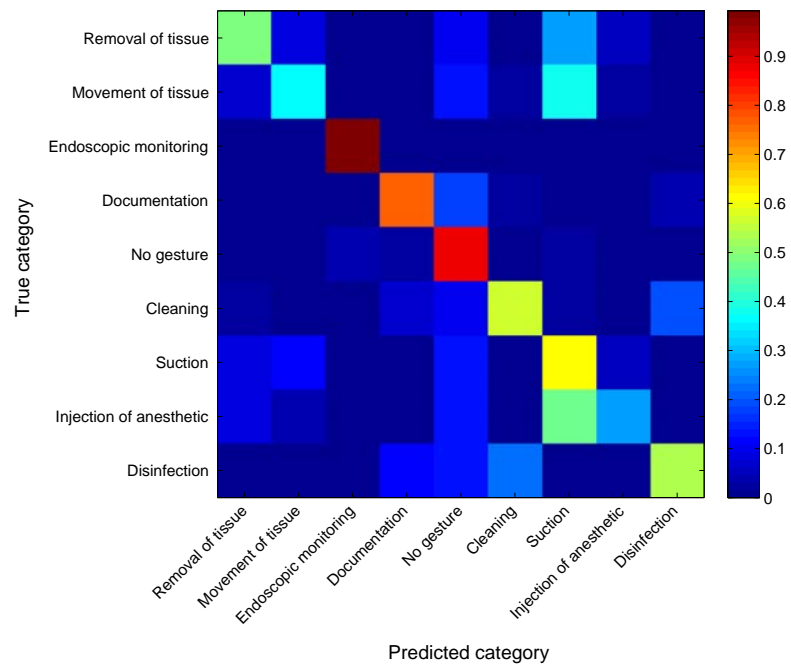
Figure 8 shows the confusion matrix of the true and predicted categories. Given a perfect prediction result, only elements on the diagonal should be different from deep blue, which represents no coincidence. The more red an element is, the higher is the coincidence of the predicted and true categories. The classification results were normalized to a range of 0–1.

The confusion matrix shows that some movements in all categories were falsely classified as another category. The gesture of moving tissue was classified as suction in 38 % of

Table 1 Gesture recognition results for the 734 surgical activities

Gesture	Accuracy in % Mean (SD)	Precision in % Mean (SD)	Recall in % Mean (SD)	No. of gesture frames in the test data
Removal of tissue	89 (6)	89 (8)	52 (24)	12,052
Movement of tissue	96 (3)	31 (25)	39 (18)	1,162
Endoscopic monitoring	99 (2)	98 (2)	99 (1)	26,796
Documentation	99 (0)	47 (21)	74 (26)	496
No gesture	93 (4)	81 (15)	83 (15)	13,127
Cleaning	98 (1)	66 (10)	59 (19)	1,247
Suction	90 (4)	37 (19)	59 (17)	4,041
Injection of anesthetic	98 (2)	23 (28)	29 (25)	606
Disinfection	99 (0)	48 (25)	51 (23)	672
Mean	96	58	60	
Median	97	53	59	
Standard deviation	3	19	14	

The accuracy was calculated for each of the $N = 12$ interventions and the mean and standard deviation (SD) of the accuracies is reported

Fig. 8 Confusion matrix showing the predicted and true categories, with *red* denoting a high coincidence and *blue* denoting a low coincidence

cases. Injection of anesthetic was recognized as suction in 47 % of cases.

Discussion

The recognition of surgical activities is a key step in the recognition of a surgical process. This concept is the basis for procedure time estimation, documentation, and automated triggering of devices. The recognition of activities is achieved

by acquiring and processing sensor data. To circumvent the need to modify instruments, a vision-based approach was chosen. We used an infrared thermal camera combined with an HTM network to classify the activities of surgical workflows.

Our system can be used to recognize surgical activities in real time. Using a standard Windows-based desktop PC, we were able to process the images and to classify the surgical activities in approximately 0.3 s. Therefore, this system can be used to recognize surgical activities online and to pro-

vide input data to surgical assistance systems and workflow management systems.

Our study demonstrated the recognition of surgical activities in infrared thermal images. We achieved a mean accuracy of 96 % and a mean recall rate of 60 %. Certain categories had a high recall rate, reaching up to 98 %, whereas other categories had rates as low as 27 %. The main divergence was between the categories of movement of tissue, suction, and injection of anesthetic. A probable cause is the limited resolution of the thermal camera. The extracted images containing the hand of the surgeon were only 50×50 pixels in size. This limited resolution is challenging for object recognition in general. In our project, it was difficult even for a human to distinguish between certain similar categories, e.g., elevator and suction use. A higher resolution will provide more detailed images. Thus, a higher recall rate is expected for the system.

The category recognized least was injection of anesthetic, possibly because of the small amount of training data. The amount of training data depends on the distribution of a gesture throughout an intervention. Injection of anesthetic, for instance, is performed only at the beginning of an intervention and only for a short period of time (10 s of an intervention running 20 min), whereas an endoscope is used nearly entirely throughout an intervention. The very skewed imbalance in the amount of training data has a disadvantage. The KNN, used as a classifier, stores the training data and categories. Thus, certain ambiguous and rarely occurring categories may be mostly classified into other categories because several categories are overtrained. However, making the amount of training data per category more balanced is not a solution. On the contrary, this balancing will reduce the overall recall rate because the variety of gestures is not learned.

The results are similar to those of other vision-based approaches. Blum et al. [22] recognized phases using video data with a recall rate of up to 77 %. Lalys et al. [23] achieved an accuracy of 95 % for the offline detection of visual cues in cataract surgeries. In another study [24], the recognition rate of activities in cataract surgeries was 64.5 %.

In contrast to the use of conventional visual cameras, thermal data provide additional information about a scene. When trying to classify the gestures of a surgeon, it is only plausible to make use of the temperature information. The clothes worn for sterility purposes allow easy extraction of the hands of the surgeon. The clothing shields the body temperature of the person, whereas the gloves provide sufficient thermal conductivity. Therefore, the hands are well distinguishable from the surroundings and background. The extraction of the hands is more complex if the background is at approximately the same temperature as the hands. This similarity may be the case, for instance, when the hands are in between the thermal camera and the operating field. Thus, a dynamic

background detection algorithm may be needed to place the camera more freely.

A HTM was chosen for object recognition because recent studies showed that hierarchical systems have advantages when invariance is demanded in vision-based object recognition [30], [31]. Additionally, in contrast to classic pattern matching methods, the memory usage and calculation times do not grow with the amount of the training/reference data. Therefore, a large amount of training images could be used for learning the network.

In the future, the application of the system to a real surgical environment needs to be investigated, including aspects such as the mounting of the camera in an OR on a rack or microscope. Additionally, the warmth of the operating field needs to be considered. The currently implemented algorithms that extract gestures rely on the fact that the hands of the surgeon are warmer than ambient areas. When the surgeon handles instruments in front of the operating field, this distinction may not be the case.

Our system was validated using one type of surgery. Further studies must be performed to estimate the feasibility of expanding this technique to general use.

Furthermore, the method of training the system is still very time-consuming. First, the software needs to extract all gestures from the training videos. Afterward, each extracted gesture needs to be labeled by a human observer. Therefore, if the procedure times are long or the variety of gestures is very high, a large amount of gestures needs to be labeled for training. In these cases, the current learning procedure is inefficient. Hence, a way of training the system semi-automatically needs to be found. Based on a recorded workflow, an HTM should be able to learn the correlation between the workflow and the images recorded by a camera.

Conclusion

Surgical processes are complex entities that rely on expressive models and data for their description. The main limitation of current vision-based recognition methods is inefficiency in online recognition because of the large amount of information generated. We have overcome this problem using infrared thermal imaging for the recognition of surgical activities. Combining an infrared thermal camera with an HTM network for the classification of activities, we obtained an online recognition rate of 96 %. This finding provides a basis for further workflow management and surgical assistance systems that demand robust recognition of surgical activities to provide situation-dependent support to the surgeon.

Acknowledgments ICCAS is funded by the German Federal Ministry of Education and Research (BMBF) in the scope of the Unternehmen

Region (Grant Number 03Z1LN12) and by the German Ministry of Economics (BMWi) in the scope of the Zentrales Innovationsprogramm Mittelstand (ZIM) (Grant Number KF2036709FO0).

Conflict of interest The authors declare that they have no conflict of interest.

References

- Archer T, Macario A (2006) The drive for operating room efficiency will increase quality of patient care. *Curr Opin Anaesthesiol* 19:171–176. doi:[10.1097/01.aco.0000192796.02797.82](https://doi.org/10.1097/01.aco.0000192796.02797.82)
- Sutherland J, van den Heuvel W-J (2006) Towards an intelligent hospital environment: adaptive workflow in the OR of the future. Proceedings of the 39th annual Hawaii international conference on system sciences, volume 05. IEEE Computer Society, Washington, DC, USA, p 100b
- Cleary K, Kinsella A, Mun SK (2005) OR 2020 workshop report: operating room of the future. *Int Congr Ser* 1281:832–838. doi:[10.1016/j.ics.2005.03.279](https://doi.org/10.1016/j.ics.2005.03.279)
- Neumuth T, Jannin P, Schlomberg J et al (2011) Analysis of surgical intervention populations using generic surgical process models. *Int J Comput Assist Radiol Surg* 6:59–71. doi:[10.1007/s11548-010-0475-y](https://doi.org/10.1007/s11548-010-0475-y)
- Neumuth T (2013) Surgical process modeling: theory, methods, and applications
- Neumuth T, Liebmann P, Wiedemann P, Meixensberger J (2012) Surgical workflow management schemata for cataract procedures. Process model-based design and validation of workflow schemata. *Methods Inf Med* 51:371–382. doi:[10.3414/ME11-01-0093](https://doi.org/10.3414/ME11-01-0093)
- Franke S, Meixensberger J, Neumuth T (2013) Intervention time prediction from surgical low-level tasks. *J Biomed Inform* 46:152–159. doi:[10.1016/j.jbi.2012.10.002](https://doi.org/10.1016/j.jbi.2012.10.002)
- Tiwari V, Dexter F, Rothman BS et al (2013) Explanation for the near-constant mean time remaining in surgical cases exceeding their estimated duration, necessary for appropriate display on electronic white boards. *Anesth Analg* 117:487–493. doi:[10.1213/ANE.0b013e31829772e9](https://doi.org/10.1213/ANE.0b013e31829772e9)
- Epstein RH, Dexter F (2012) Mediated interruptions of anaesthesia providers using predictions of workload from anaesthesia information management system data. *Anaesth Intensive Care* 40:803–812
- Lin HC, Shafran I, Yuh D, Hager GD (2006) Towards automatic skill evaluation: detection and segmentation of robot-assisted surgical motions. *Comput Aided Surg* 11:220–230. doi:[10.3109/10929080600989189](https://doi.org/10.3109/10929080600989189)
- Judkins TN, Oleynikov D, Stergiou N (2009) Objective evaluation of expert and novice performance during robotic surgical training tasks. *Surg Endosc* 23:590–597. doi:[10.1007/s00464-008-9933-9](https://doi.org/10.1007/s00464-008-9933-9)
- Reiley CE, Lin HC, Varadarajan B et al (2008) Automatic recognition of surgical motions using statistical modeling for capturing variability. *Stud Health Technol Inform* 132:396
- Vankipuram M, Kahol K, Cohen T, Patel VL (2009) Visualization and analysis of activities in critical care environments. *AMIA Annu Symp Proc* 2009:662–666
- Bouarfa L, Jonker PP, Dankelman J (2009) Surgical context discovery by monitoring low-level activities in the OR
- Neumuth T, Meissner C (2012) Online recognition of surgical instruments by information fusion. *Int J Comput Assist Radiol Surg* 7:297–304. doi:[10.1007/s11548-011-0662-5](https://doi.org/10.1007/s11548-011-0662-5)
- Meißner C, Neumuth T (2012) RFID-based surgical instrument detection using Hidden Markov models. *Biomed Tech (Berl)*. doi:[10.1515/bmt-2012-4047](https://doi.org/10.1515/bmt-2012-4047)
- Kranzfelder M, Zywitzka D, Jell T et al (2012) Real-time monitoring for detection of retained surgical sponges and team motion in the surgical operation room using radio-frequency-identification (RFID) technology: a preclinical evaluation. *J Surg Res* 175:191–198. doi:[10.1016/j.jss.2011.03.029](https://doi.org/10.1016/j.jss.2011.03.029)
- Ahmadi S-A, Padoy N, Heining SM et al (2008) Introducing wearable accelerometers in the surgery room for activity detection. 7. Jahrestagung der Deutschen Gesellschaft fuer Computer-und Roboter-Assistierte Chirurgie (CURAC 2008)
- Lester J, Choudhury T, Kern N et al (2005) A hybrid discriminative/generative approach for modeling human activities. In: Proceedings of the international joint conference on artificial intelligence (IJCAI), pp 766–772
- Klank U, Padoy N, Feussner H, Navab N (2008) Automatic feature generation in endoscopic images. *Int J CARS* 3:331–339. doi:[10.1007/s11548-008-0223-8](https://doi.org/10.1007/s11548-008-0223-8)
- Blum T, Feußner H, Navab N (2010) Modeling and segmentation of surgical workflow from laparoscopic video. In: Jiang T, Navab N, Pluim J, Viergever M (eds) Medical image computing and computer-assisted intervention—MICCAI 2010. Springer, Berlin, pp 400–407
- Lalys F, Riffaud L, Bouget D, Jannin P (2011) An application-dependent framework for the recognition of high-level surgical tasks in the OR. In: Fichtinger G, Martel A, Peters T (eds) Medical image computing and computer-assisted intervention—MICCAI 2011. Springer, Berlin, pp 331–338
- Lalys F, Bouget D, Riffaud L, Jannin P (2013) Automatic knowledge-based recognition of low-level tasks in ophthalmological procedures. *Int J Comput Assist Radiol Surg* 8:39–49. doi:[10.1007/s11548-012-0685-6](https://doi.org/10.1007/s11548-012-0685-6)
- Haro BB, Zappella L, Vidal R (2012) Surgical gesture classification from video data. In: Ayache N, Delingette H, Golland P, Mori K (eds) Medical image computing and computer-assisted intervention—MICCAI 2012. Springer, Berlin, pp 34–41
- Appenrodt J, Al-Hamadi A, Michaelis B (2010) Data gathering for gesture recognition systems based on single color-, stereo color- and thermal cameras. *Int J Signal Process Image Process Pattern Recognit* 3:37–50
- Hawkins J, George D (2006) Hierarchical temporal memory: concepts, theory, and terminology
- Hawkins J, Blakeslee S (2007) On intelligence. Macmillan, New York
- Kapuscinski T (2010) Using hierarchical temporal memory for vision-based hand shape recognition under large variations in hand's rotation. In: Rutkowski L, Scherer R, Tadeusiewicz R et al (eds) Artificial intelligence and soft computing. Springer, Berlin, pp 272–279
- Kapuscinski T, Wysocki M (2009) Using hierarchical temporal memory for recognition of signed polish words. In: Kurzynski M, Wozniak M (eds) Computer recognition systems 3. Springer, Berlin, pp 355–362
- Bengio Y (2009) Learning deep architectures for AI. *Found Trends Mach Learn* 2:1–127. doi:[10.1561/22000000006](https://doi.org/10.1561/22000000006)
- Bouvier J, Rosasco L, Poggio T (2009) On invariance in hierarchical models. *Adv Neural Inf Process Syst* 22:162–170

Michael Unger*, Adrian Franke and Claire Chalopin

Automatic depth scanning system for 3D infrared thermography

DOI 10.1515/cdbme-2016-0162

Abstract: Infrared thermography can be used as a pre-, intra- and post-operative imaging technique during medical treatment of patients. Modern infrared thermal cameras are capable of acquiring images with a high sensitivity of 10 mK and beyond. They provide a planar image of an examined 3D object in which this high sensitivity is only reached within a plane perpendicular to the camera axis and defined by the focus of the lens. Out of focus planes are blurred and temperature values are inaccurate. A new 3D infrared thermography system is built by combining a thermal camera with a depth camera. Multiple images at varying focal planes are acquired with the infrared camera using a motorized system. The sharp regions of individual images are projected onto the 3D object's surface obtained by the depth camera. The system evaluation showed that deviation between measured temperature values and a ground truth is reduced with our system.

Keywords: 3D scene; depth of field; sharpness; thermal imaging.

1 Introduction

Infrared thermography was introduced in the medical area already in the 1960s [1]. It is employed for diagnosis and monitoring of diseases involving temperature differences. Some applications are the detection of tumors [2, 3] or the monitoring of cardiovascular diseases [4, 5]. Moreover, because acquisition of data is performed contactless, thermography was brought in surgery for pre-operative planning, as intra-operative assistance tool and for post-operative monitoring of surgical outcome. Applications were mostly reported in neurosurgery [6–8] and in plastic

surgery [9, 10]. Furthermore, since body temperature is correlated with tissue perfusion, identification and monitoring of skin transplants can be performed with this imaging technique [11, 12].

Recent technical developments apply thermal imaging onto 3D scenes for visualization purposes [13]. This technique was presented for medical applications too [14–16]. However, thermal cameras possess a very small depth of field, especially at small distances between camera and object [17]. Soldan [18] extended the depth of field by combining multiple thermal images of the same scene acquired with varying focuses. The optimal focus for an object is chosen by selecting a focus measure function (FMF). The FMF yields a minimum or maximum value at optimum. But good results require selecting an optimal FMF and its parameters for a given scene.

To overcome this disadvantage we combined an infrared thermal camera and a depth camera. The latter records a 3D surface of the examined object. Multiple thermal images of the scene are acquired with the infrared camera at varying focus settings. The optimal measurement is selected as a function of its depth in the 3D scene. Sharp parts of each thermal image are projected on the 3D object surface in order to reconstruct a sharp 3D thermal scene. An automatic focus control system was implemented with the future goal to use the device in the operating room.

2 3D thermographic imaging system

Then imaging system consisting of an infrared thermal camera Optris PI450 and a Microsoft Kinect V2, providing depth and visual information (Figure 1). The thermal camera has a spatial resolution of 382×288 pixels and a thermal sensitivity of 40 mK. The Kinect V2 provides a depth image with a spatial resolution of 512×424 pixels and a visual image of 1920×1080 pixels. The depth resolution is approximately 1 mm in a range of 0.5 m to 4 m.

The sharpness of the thermal image needs to be adjusted manually. To overcome this, we outfitted the

*Corresponding author: Michael Unger, University of Leipzig, Innovation Center Computer Assisted Surgery, Semmelweisstr. 14, D-04103 Leipzig, E-mail: michael.unger@iccas.de

Adrian Franke: Ilmenau University of Technology, E-mail: adrian.franke@tu-ilmenau.de

Claire Chalopin: University of Leipzig, Innovation Center Computer Assisted Surgery, E-mail: claire.chalopin@iccas.de

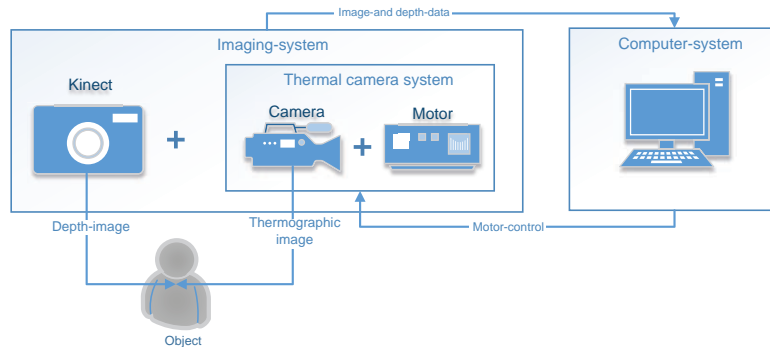


Figure 1: The thermographic imaging system consists of a thermal camera and depth camera. A motor focus for the thermal camera allows for automatic image acquisition at different focal planes. A computer system processes the data.

camera with a drive for focus control. The hardware consists of a gear motor with a rotary encoder for position measurement which is controlled by an Arduino board. A firmware was developed providing basic functions for referencing the focus as well as getting and setting the focus position.

A software developed by us retrieves the temperature information and a depth image via provided vendor software. The thermal images are acquired using the Optris PI Connect which supplies the data for the inter-process communication via a dynamic link library. The Kinect for Windows SDK is used to acquire the depth and RGB images from the Kinect camera. After reconstructing the all-in-focus image, the 3D scene with applied thermal image mapping is rendered using the Kinect Fusion API.

plane. The measurement was done by moving a checkerboard until it was displayed sharply and reading the corresponding object distance from the depth image.

2.1.2 Camera calibration

To be able to combine the spatial data of the depth camera and the temperature data of the thermal camera, the optical intrinsic (lens specific) and extrinsic parameters of the components must be calculated. For this process a known geometric pattern that is visible in both image modalities is needed. We used a checkerboard pattern which had alternating tiles removed (Figure 2). The removed tiles were clearly visible in both the depth and thermal image.

2.1 Calibration of the system components

The components of the 3D thermographic imaging system must be calibrated in order to combine the different imaging modalities. The calibration process is described in detail in the following sections.

2.1.1 Calibration of the focus

Changing the focus of the thermal camera defines which objects at a certain distance to the camera will be displayed sharply. For automating the image acquisition process, the dependency between focus setting and the focal plane needs to be known. Therefore, the focus was referenced (zero position) by driving it to its end position. Following, the characteristic curve was determined by incrementally setting the focus and measuring the corresponding focal

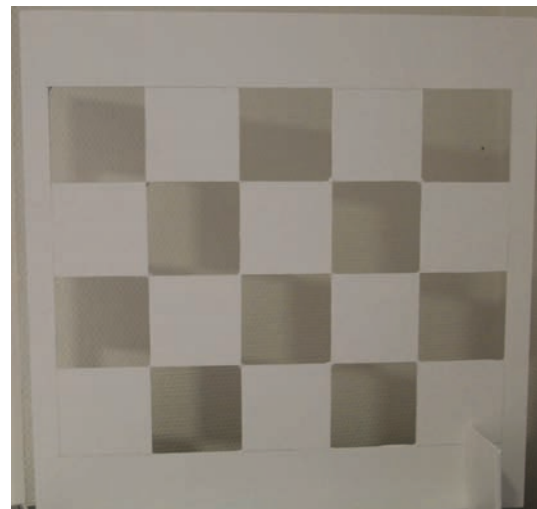


Figure 2: Checker board uses in the calibration process.

Firstly, the intrinsic parameters of the thermal camera were calculated. The intrinsic parameters of the depth camera are stored in its firmware. Secondly, the extrinsic parameters describing the spatial relation between the cameras were obtained. Using the resulting transformation matrix, the thermal image can be projected onto the 3D scene retrieved by the depth camera.

2.2 Depth scanning

To improve the image quality, sharp parts of multiple thermal images are combined to an overall sharp image. Therefore, images at multiple focal planes are acquired. Points of the 3D surface acquired with the depth camera become the temperature value in the corresponding thermal image obtained using the transformation between thermal and depth images.

2.3 System evaluation

To evaluate the system an object which is visible in the depth and thermal data was constructed. We mounted LED stripes into grids onto a plane board. Three boards were positioned to focal planes at a distance of 500, 1000, 1500 mm. Each board contained 120 LEDs.

The current flowing through the LEDs causes heating which was used to evaluate the image quality. If the plane containing the LEDs is out of focus it gets blurred. This blurring leads to a reduced temperature of the LED measured in the thermal image. The LEDs were heated for half an hour to reach a steady state. Then a manually focused thermal image of each board was acquired. These images were used as a ground truth.

Secondly, our system reconstructed an overall sharp image using depth scanning (Figure 3). We calculated the temperature difference between the ground truth and our algorithm. If the correct focus setting corresponding to the

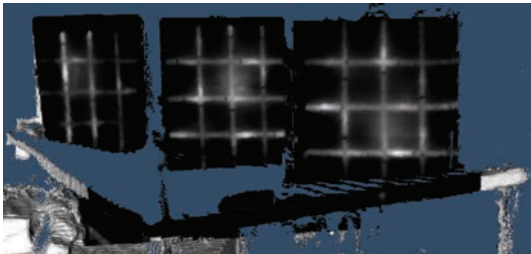


Figure 3: Reconstructed 3D scene with applied thermal map.

Table 1: Temperature deviation due to blurring.

	ΔT with depth scanning (K)		ΔT without depth scanning (K)	
	mean	std	mean	std
Board 1 (near)	-2.45	0.36	-16.80	0.21
Board 2 (mid)	-0.56	0.19	-0.36	0.13
Board 3 (far)	-1.31	0.24	-5.47	0.30

thermal pixel was selected the temperature difference is expected to be zero. The depth scanning algorithm was compared to an image with the focus set to the middle board.

3 Results

When using depth scanning, the temperature deviation due to blurring is reduced (Table 1). The biggest improvement was achieved at near distance to the object. At far distances the negative effects of the small field of depth have less impact.

4 Discussion and conclusion

We showed that reconstructing an all-in-focus thermal image improves the image quality and therefore the accuracy of the temperature measurement. The temperature deviation induced by blurring was reduced but was still up to 2.45 K.

Remaining errors may be caused by the rather simple model used for the camera calibration. Adjusting the focus causes a change in the focal length parameter which was assumed fix. This dependency needs to be added to the calibration process.

[18] improved the image quality by calculating an all-in-focus thermal image by applying algorithms developed for visual images. This process requires adjusting parameters depending on the scene. By using a depth camera no parameters need to be adjusted, but more hardware is needed and the calibration process is more complex.

Further evaluation of the imaging system is needed to assess the impact on the image quality in medical use cases.

Author's Statement

Research funding: Sponsored by the Federal Ministry of Education and Research. Conflict of interest: Authors state

no conflict of interest. Material and methods: Informed consent: Informed consent is not applicable. Ethical approval: The conducted research is not related to either human or animal use.

References

- [1] Ring EF, Ammer K. Infrared thermal imaging in medicine. *Physiol Meas.* 2012;33:R33–46.
- [2] Gerasimova E, Audit B, Roux SG, Khalil A, Gileva O, Argoul F, et al. Wavelet-based multifractal analysis of dynamic infrared thermograms to assist in early breast cancer diagnosis. *Front Physiol.* 2014;5(Article 176):1–11.
- [3] Çetingül MP, Herman C. Quantification of the thermal signature of a melanoma lesion. *Int J Therm Sci.* 2011;50:421–31.
- [4] Szentkuti A, Kavanagh HS, Grazio S. Infrared thermography and image analysis for biomedical use. *Period Biol.* 2011;113: 385–92.
- [5] Jin C, Yang Y, Xue ZJ, Liu KM, Liu J. Automated analysis for screening knee osteoarthritis using medical infrared thermography. *J Med Biol Eng.* 2013;33:471–7.
- [6] Kateb B, Yamamoto V, Yu C, Grundfest W, Gruen JP. Infrared thermal imaging: a review of literature and case report. *NeuroImage.* 2009;47:T154–62.
- [7] Steiner G, Sobottka SB, Koch E, Schackert G, Kirsch M. Intraoperative imaging of cortical cerebral perfusion by time-resolved thermography and multivariate data analysis. *J Biomed Opt.* 2011;16:1–6.
- [8] Rathmann P, Lindner D, Halama D, Chalopin C. Dynamische Infrarot-Thermographie (DIRT) zur Darstellung der Kopfhautdurchblutung bei neurochirurgischen Eingriffen, in Tagungsband der 14. Jahrestagung der Deutschen Gesellschaft für Computer und Roboterassistierte Chirurgie (CURAC), Bremen, 2015, pp. 17–19.
- [9] de Weerd L, Weum S, Mercer JB. The value of dynamic infrared thermography (DIRT) in perforatorselection and planning of free DIEP flaps. *Ann Plast Surg.* 2009;63:274–9.
- [10] Chubb DP, Taylor GI, Ashton MW. True and “Choke” anastomoses between perforator angiosomes: part II. Dynamic thermographic identification. *Plast Reconstr Surg.* 2013;132:1457–64.
- [11] Lohman RF, Ozturk CN, Ozturk C, Jayaprakash V, Djohan R. An analysis of current techniques used for intraoperative flap evaluation. *Ann Plast Surg.* 2015;75:679–85.
- [12] Just M, Chalopin C, Unger M, Halama D, Neumuth T, Dietz A, et al. Monitoring of microvascular free flaps following oropharyngeal reconstruction using infrared thermography: first clinical experiences. *Eur Arch Otorhinolaryngol.* 2015;273:1–9.
- [13] Barone S, Paoli A, Razonale AV. A biomedical application combining visible and thermal 3D imaging. presented at the XVIII Congreso internacional de Ingeniería Grafica, Barcelona, 2006.
- [14] Spalding SJ, Kwok CK, Boudreau R, Enama J, Lunich J, Huber D, et al. Three-dimensional and thermal surface imaging produces reliable measures of joint shape and temperature: a potential tool for quantifying arthritis. *Arthritis Res Ther.* 2008;10:R10.
- [15] Grubisic I, Gjenero L, Lipic T, Sovic I, Skala T. Medical 3D thermography system. *Period Biol.* 2011;113:401–6.
- [16] Chen CY, Yeh CH, Chang BR, Pan JM. 3D reconstruction from IR thermal images and reprojective evaluations. *Math Probl Eng.* 2015;2015:8.
- [17] Schuster N, Franks J. Depth of field in modern thermal imaging. Presented at the SPIE Defense+ Security. International Society for Optics and Photonics, 2015, pp. 94520J–94520J–11.
- [18] Soldan S. On extended depth of field to improve the quality of automated thermographic measurements in unknown environments. *Quant Infrared Thermogr J.* 2012;9:135–50.

Summary

Dissertation zur Erlangung des akademischen Grades

Dr. rer. med.

Developments of Infrared Thermography-based Tools to Assist Surgical Procedures and Workflow

eingereicht von

Michael Unger, M.Sc.

angefertigt an der

Universität Leipzig, Medizinische Fakultät, Innovation Center Computer Assisted Surgery (ICCAS)

betreut von

Prof. Thomas Neumuth

April 2022

Infrared thermography (IRT) has been used for medical applications since the 1960s. The means of non-invasive temperature measurement made infrared thermography an interesting technology for the detection of diseases causing changes in metabolic activity and thus in temperature. Technological advantages lead to improvements like higher thermal sensitivity, higher resolution, as well as smaller and cheaper systems which expanded the field of research. The field of research in this work investigated previously uncovered applications and technological improvements of thermography for use in surgical environments.

This work investigated a use case to support surgical procedures by using IRT for diagnostic purposes. IRT has been widely used in the medical domain for the diagnosis of diseases. Because physiological processes have an impact on tissue temperature, thermal imaging can be used to contactless measure the skin surface temperature. For example, IRT was used to monitor the skin temperature [Cha15], to detect skin cancer [PH11], breast tumours [Omr16; Vre13], inflammation [Den10] and vascular disorders [Bag09; LEP17].

In reconstructive surgery, the transfer of microvascular tissue is a routinely used method for covering defects caused by injuries, tumor removal, or malformations. These transplants include skin, subcutaneous tissue, and blood vessels. The location of the blood vessels supplying the tissue (perforator vessels) needs to be known during the planning of the operation to avoid necrosis after transplantation. Imaging techniques to visualize the perforator vessels are digital subtraction angiography (DSA), computed tomography angiography (CTA), and mag-

netic resonance angiography (MRA) which are used pre-operatively. These methods provide a high image quality but require the administration of a contrast agent or exposing the patient to radiation. The selection of the donor flap is made during the intervention in the operating room (OR) because the flap size depends on the actual defect [WW10]. Intra-operatively used imaging techniques are doppler ultrasound (Doppler-US) and indocyanine green angiography (ICG-A). Doppler-US is non-invasive but the quality of the perforator identification depends on the skill of the surgeon. ICG-A is the current standard, but the administration of a fluorescent dye impacts the ease of use and isn't compatible with specific diseases. DeWeerd et al. used IRT to visually locate perforator vessels by qualitative assessment of thermograms of the deep inferior epigastric perforator (DIEP) flap [dWWM12b]. However, perforator locations were only determined manually which requires experience and examination time.

In this work, a thermography-based system to automatically locate the perforator vessels was designed, evaluated, and published in the article *Automatic detection of perforator vessels using IRT in reconstructive surgery*. The system consists of a thermal camera, a computer, and custom-developed software. As the perforators correspond to hot spots in the thermogram, an algorithm to find local hot spots in the thermal image was developed. A Gaussian blur filter was applied to reduce noise, followed by a local maximum search. The filter kernel size can be adjusted by the user to set the detection sensitivity. For the evaluation, the thermal camera was used to acquire the temperature variations of the skin surface of the DIEP flap of 20 volunteers. The volunteers were placed in an intra-operative setting on the OR table. The detected perforator centers were compared to the manual labeling performed by clinicians. The perforator was classified as detected if the distance between the manually labeled perforator center and the center detected by the algorithm was less than 10 pixels (≈ 5 mm). The algorithm performance was evaluated by calculating recall and precision and F measure (harmonic mean of precision and recall). The best F measure of 0.833 is reached for a kernel size of 17. For this parameter value, the median recall is 0.907 and the median precision is 0.80. The kernel size can be chosen by the clinician to optimize the detection performance for specific patients and regions under examination. Although the algorithm performance varied, no statistically significant differences regarding specific parameters such as gender, age, or daily sports activity could be measured within the cohort of the conducted study. Furthermore, the algorithm was only evaluated for the region of the DIEP flap. More studies are necessary to assess the performance of typical donor flap regions.

Thermography is advantageous to commonly used imaging techniques because it is non-invasive. As opposed to CTA or ICG-A no contrast agent needs to be administered which nullifies the side effects. Furthermore, contrast agent-based imaging can't be repeated without

restrictions due to its proliferation in the body which reduces the quality of subsequent images. In contrast, the use of thermography as presented in this work is not limited in this regard. The detection of hot spots in real-time and the compact system size makes it a versatile tool for use inside and out of the OR whereas CT angiography can only be acquired preoperatively.

While using thermography for the diagnosis of diseases is obvious, IRT can also be used to improve technical systems in the OR. Hereby, a broadly investigated field of research is the improvement of processes and workflows in the OR. To improve the processes, for example, by automating tedious and repetitive tasks, knowledge of the ongoing tasks and activities in the OR is needed. The classification of surgical activities is a vital step as workflow management engines require knowledge of the situation in the OR. Surgical activities can be automatically deducted from sensor data by analyzing the motion of the surgeon using accelerometers or equivalent wearable devices [Ahm08; Les05; NM12] and RFID tags attached to surgical instruments and personnel [BJD09; Kra12; MN12; NM12; Van09]. As these approaches require the modification of surgical instruments or wearing special equipment, barriers to establishing such technologies in the OR is quite high. Alternatively, surgical processes can be identified by analyzing video data in endoscopic procedures [BFN10; Bou17; HZV12; Kla08; Lal13; Lal11] or cameras monitoring the surgical team [Bha07].

One of the main challenges of vision-based methods for the recognition of surgical activities is the extraction of the foreground object, e.g. the surgical instrument. Changes in the background image, varying lighting conditions, and image quality make robust activity recognition all the more difficult. Thermal imaging extends the information space beyond the visible spectrum. The hands of the surgeon have a higher temperature than the background scene. Therefore, temperature information can be used to extract regions of interest and recognize surgical activities. The manuscript *Vision-based online recognition of surgical activities* investigated the development and evaluation of a system that is capable of recognizing surgical activities by analyzing thermal video data. A thermal camera was used to acquire images of a surgical scene and the regions of interest, i.e. the hand of the surgeon were extracted via thresholding. In the segmented images, a blob detector was applied. A hierarchical temporal memory (HTM) combined with a k-nearest neighbor algorithm was used for gesture recognition. This approach was evaluated in a simulated functional endoscopic sinus surgery. 12 videos (~ 20 min each) of three different workflows representing surgeries were recorded. The system was trained using manually labeled gestures in 9 classes and was validated with leave-one-out cross-validation.

The system was capable to classify images in real-time providing input for surgical assistance systems and workflow management systems. The recognition accuracy of 96 % with precision

and recall rates of approximately 60 % was similar to other vision-based approaches [BFN10; Lal11; Lal13]. The recall rates varied between the classes (29 % to 99 %). A probable cause is the limited resolution of only 50 x 50 pixels of the objects impedes the correct gesture classification, especially if the instruments are held by the surgeon, and therefore the hand poses, differ only slightly. Today commercially available cameras offer 17 times the spatial resolution of the used camera which enables depicting more details of the scene. Further investigations are needed to assess how much an increased resolution improves the recognition. HTM was a state-of-the-art method at the time of the publication of the manuscript. Since then, many advances in machine learning, especially deep learning, were made. Hence, the proposed approach may be improved using the latest machine learning methods. But using machine learning approaches in general and deep learning especially requires a huge amount of training data that needs to be annotated manually to keep a clean training data set.

Although thermal cameras were already introduced in the medical field in the 1960s, technical advancements were mostly made to reduce the size of the devices, increase the resolution of the acquired images and increase the thermal sensitivity. Due to physical constraints, it's not possible to reduce the size of the imaging sensor. Therefore, thermal cameras have a small depth of field, especially at small distances between camera and object [SF15]. Hence, to acquire sharp images the focal plane must be aligned to the region of interest. Blurred images lead to loss of information and thus may reduce the performance of image processing algorithms. The impact of this loss of information is depending on the application. Soldan extended the depth of field by combining multiple thermal images of the same scene acquired with varying focuses [Sol12]. The optimal focus for an object is chosen by selecting a focus measure function (FMF). The FMF yields a minimum or maximum value at optimum. But good results require selecting an optimal FMF and its parameters for a given scene. To overcome this problem a method to reconstruct an all-in-focus image was proposed and published under the title *Automatic depth scanning system for 3D infrared thermography*. A thermal camera was combined with a depth camera and a drive to adjust the focus. This enables taking images at variable depths. Software controls and synchronizes the image acquisition with the depth and thermal camera. Both cameras were registered to each other which enables the mapping of the pixels of the thermal image to a certain depth. A system evaluation was conducted by placing heated objects at different distances. The reconstruction of an all-in-focus image reduced the temperature deviation over all distances. Although the temperature measurement could be vastly improved, the measurement error was still up to 2.5 K. The remaining error may be caused by the simplified calibration model and can be further reduced by improving the calibration process and integrating the

approach into a single device. The proposed method enables applications that are based on accurate temperature measurements for objects at varying depths without manually adjusting the focus. The reconstruction of the all-in-focus image requires the acquisition of multiple thermal images. Therefore, this method is not applicable for dynamic or real-time analysis and has its limitations regarding usability.

3.1 Conclusions and Outlook

Thermography can be used for diagnosis as well as part of technical systems providing support in the OR. There are limitations caused by physical constraints which impede broad and easy use. Thermal cameras possess a small depth of field which leads to blurred images when the focus isn't set optimal. Adjusting the focus manually is cumbersome and impacts usability. Further improvements are necessary to provide systems that are as easy to use as RGB cameras.

Properties like the resolution and sensitivity of thermal cameras improved over time enabling the detection of the smallest temperature differences which enables using IRT for the detection of blood vessels beneath the skin. By providing software-based tools locating perforator vessels becomes easier and is less impacted by the skill of the clinician. In this work, only static images were analyzed to detect the locations of the perforator vessels. Further enhancements can be made by combining multiple static images to improve the recognition robustness over time or analyzing the thermograms over time. By exposing the tissue to a cold challenge and analyzing the reheating of the skin surface, it might be possible to estimate the strength of the underlying perforators. To further improve this approach, thermal imaging could be combined with hyperspectral imaging (HSI). HSI describes the number of modalities used for imaging. Whereas IRT uses only one (broad) spectrum ranging from $8\text{ }\mu\text{m}$ to $14\text{ }\mu\text{m}$ and visible imaging uses three spectra, red (650 nm .. 750 nm), green (490 nm .. 575 nm), and blue (420 nm .. 490 nm), HSI uses 100 spectra and more ranging from 400 nm to 1100 nm. Hence, HSI is covering the visible and near-infrared spectral range. By analyzing the spectral distribution of light reflected from the skin surface, various parameters can be calculated. For example, HSI was used to measure tissue oxygenation (StO₂), perfusion-(NIR Perfusion Index), organ hemoglobin (OHI), and tissue water index (TWI) for the measurement of ischemic conditioning effects of the gastric conduit during esophagectomy [Köh19]. In colorectal surgery, HSI was used for the assessment of the best possible perfusion and ideal anastomotic area by visualizing the tissue perfusion before and after the separation of the marginal artery [Jan19]. Initial studies investigating the feasibility of using HSI for perforator identification are inconclusive [Goe20; Nis21]. Therefore, the approach to use HSI as an adjuvant imaging modality to further improve the assessment of the perforator locations must be investigated further.

References

- [Dur16] H. Durrani. “Healthcare and Healthcare Systems: Inspiring Progress and Future Prospects”. In: *mHealth* 2 (Feb. 2, 2016). ISSN: 2306-9740. DOI: 10.3978/j.issn.2306-9740.2016.01.03. pmid: 28293581.
- [WHO21] WHO. *Global Health Expenditure Database*. 2021. URL: https://apps.who.int/nha/database/Regional_Averages/Index/en (visited on 02/19/2021).
- [Sta21a] Statistisches Bundesamt (Destatis). *Gesundheitsausgaben: Deutschland*. 2021. URL: <https://www-genesis.destatis.de/genesis/online?levelindex=2&levelid=1613727505068> (visited on 02/19/2021).
- [Sta21b] Statistisches Bundesamt (Destatis). *Kosten Der Krankenhäuser Nach Bundesländern*. 2021. URL: <https://www.destatis.de/DE/Themen/Gesellschaft-Umwelt/Gesundheit/Krankenhaeuser/Tabellen/kosten-krankenhaeuser-bl.html> (visited on 02/19/2021).
- [Wea06] D. Weatherall, B. Greenwood, H. L. Chee, and P. Wasi. “Science and Technology for Disease Control: Past, Present, and Future”. In: *Disease Control Priorities in Developing Countries*. Ed. by D. T. Jamison, J. G. Breman, A. R. Measham, G. Alleyne, M. Claeson, D. B. Evans, P. Jha, A. Mills, and P. Musgrove. 2nd ed. Washington (DC): World Bank, 2006. ISBN: 978-0-8213-6179-5. pmid: 21250320.
- [GG11] F. Guerriero and R. Guido. “Operational Research in the Management of the Operating Theatre: A Survey”. In: *Health Care Management Science* 14.1 (Mar. 1, 2011), pp. 89–114. ISSN: 1572-9389. DOI: 10.1007/s10729-010-9143-6.
- [SvdH06] J. Sutherland and W.-J. van den Heuvel. “Towards an Intelligent Hospital Environment: Adaptive Workflow in the OR of the Future”. In: *Proceedings of the 39th Annual Hawaii International Conference on System Sciences - Volume 05*. HICSS ’06. Washington, DC, USA: IEEE Computer Society, 2006, 100b. ISBN: 0-7695-2507-5. DOI: 10.1109/HICSS.2006.494.
- [FMN15] S. Franke, J. Meixensberger, and T. Neumuth. “Multi-Perspective Workflow Modeling for Online Surgical Situation Models”. In: *Journal of Biomedical Informatics* 54 (Apr. 1, 2015), pp. 158–166. ISSN: 1532-0464. DOI: 10.1016/j.jbi.2015.02.005.
- [Neu09] T. Neumuth, P. Jannin, G. Strauss, J. Meixensberger, and O. Burgert. “Validation of Knowledge Acquisition for Surgical Process Models”. In: *Journal of the*

-
- American Medical Informatics Association* 16.1 (Jan. 1, 2009), pp. 72–80. ISSN: 1067-5027. DOI: 10.1197/jamia.M2748.
- [Neu11] T. Neumuth, P. Jannin, J. Schlomberg, J. Meixensberger, P. Wiedemann, and O. Burgert. “Analysis of Surgical Intervention Populations Using Generic Surgical Process Models”. In: *International Journal of Computer Assisted Radiology and Surgery* 6.1 (Jan. 1, 2011), pp. 59–71. ISSN: 1861-6429. DOI: 10.1007/s11548-010-0475-y.
- [BJD09] L. Bouarfa, P. Jonker, and J. Dankelman. *Surgical Context Discovery by Monitoring Low-Level Activities in the OR*. MICCAI Workshop on Modeling and Monitoring of Computer Assisted Interventions, M2CAI. 2009.
- [Kra12] M. Kranzfelder, D. Zywitza, T. Jell, A. Schneider, S. Gillen, H. Friess, and H. Feussner. “Real-Time Monitoring for Detection of Retained Surgical Sponges and Team Motion in the Surgical Operation Room Using Radio-Frequency-Identification (RFID) Technology: A Preclinical Evaluation”. In: *The Journal of surgical research* 175.2 (June 15, 2012), pp. 191–198. ISSN: 1095-8673. DOI: 10.1016/j.jss.2011.03.029. pmid: 21571315.
- [MN12] C. Meißner and T. Neumuth. “RFID-Based Surgical Instrument Detection Using Hidden Markov Models”. In: *Biomedizinische Technik. Biomedical engineering* (Aug. 31, 2012). ISSN: 1862-278X. DOI: 10.1515/bmt-2012-4047. pmid: 22945108.
- [NM12] T. Neumuth and C. Meissner. “Online Recognition of Surgical Instruments by Information Fusion”. In: *International journal of computer assisted radiology and surgery* 7.2 (Mar. 2012), pp. 297–304. ISSN: 1861-6429. DOI: 10.1007/s11548-011-0662-5. pmid: 22005841.
- [Van09] M. Vankipuram, K. Kahol, T. Cohen, and V. L. Patel. “Visualization and Analysis of Activities in Critical Care Environments”. In: *AMIA ... Annual Symposium proceedings / AMIA Symposium. AMIA Symposium 2009* (2009), pp. 662–666. ISSN: 1942-597X. pmid: 20351937.
- [Miy09] F. Miyawaki, T. Tsunoi, Hiromi Namiki, Takashi Yaginuma, K. Yoshimitsu, D. Hashimoto, and Y. Fukui. “Development of Automatic Acquisition System of Surgical-Instrument Informantion in Endoscopic and Laparoscopic Surgey”. In: *2009 4th IEEE Conference on Industrial Electronics and Applications*. 2009 4th IEEE Conference on Industrial Electronics and Applications. May 2009, pp. 3058–3063. DOI: 10.1109/ICIEA.2009.5138763.

-
- [Kra13] M. Kranzfelder, C. Staub, A. Fiolka, A. Schneider, S. Gillen, D. Wilhelm, H. Friess, A. Knoll, and H. Feussner. “Toward Increased Autonomy in the Surgical OR: Needs, Requests, and Expectations”. In: *Surgical Endoscopy* 27.5 (May 1, 2013), pp. 1681–1688. ISSN: 1432-2218. DOI: 10.1007/s00464-012-2656-y.
- [Ahm08] S.-A. Ahmadi, N. Padoy, S. M. Heining, H. Feussner, M. Daumer, and N. Navab. “Introducing Wearable Accelerometers in the Surgery Room for Activity Detection”. In: *7. Jahrestagung Der Deutschen Gesellschaft Fuer Computer-Und Roboter-Assistierte Chirurgie (CURAC 2008)*. Leipzig, Germany, Sept. 2008.
- [Les05] J. Lester, T. Choudhury, N. Kern, G. Borriello, and B. Hannaford. “A Hybrid Discriminative/Generative Approach for Modeling Human Activities”. In: *In Proc. of the International Joint Conference on Artificial Intelligence (IJCAI)*. 2005, pp. 766–772.
- [Mei14] C. Meißner, J. Meixensberger, A. Pretschner, and T. Neumuth. “Sensor-Based Surgical Activity Recognition in Unconstrained Environments”. In: *Minimally Invasive Therapy & Allied Technologies* 23.4 (Aug. 1, 2014), pp. 198–205. ISSN: 1364-5706. DOI: 10.3109/13645706.2013.878363.
- [GDN15] B. Glaser, S. Dänzer, and T. Neumuth. “Intra-Operative Surgical Instrument Usage Detection on a Multi-Sensor Table”. In: *International Journal of Computer Assisted Radiology and Surgery* 10.3 (Mar. 1, 2015), pp. 351–362. ISSN: 1861-6429. DOI: 10.1007/s11548-014-1066-0.
- [AR11] J. Aggarwal and M. Ryoo. “Human Activity Analysis: A Review”. In: *ACM Computing Surveys* 43.3 (Apr. 29, 2011), 16:1–16:43. ISSN: 0360-0300. DOI: 10.1145/1922649.1922653.
- [BFN10] T. Blum, H. Feußner, and N. Navab. “Modeling and Segmentation of Surgical Workflow from Laparoscopic Video”. In: *Medical Image Computing and Computer-Assisted Intervention ? MICCAI 2010*. Ed. by T. Jiang, N. Navab, J. Pluim, and M. Viergever. Vol. 6363. Lecture Notes in Computer Science. Springer Berlin / Heidelberg, 2010, pp. 400–407. ISBN: 978-3-642-15710-3.
- [Bou17] D. Bouget, M. Allan, D. Stoyanov, and P. Jannin. “Vision-Based and Marker-Less Surgical Tool Detection and Tracking: A Review of the Literature”. In: *Medical Image Analysis* 35 (Jan. 1, 2017), pp. 633–654. ISSN: 1361-8415. DOI: 10.1016/j.media.2016.09.003.

-
- [HZV12] B. B. Haro, L. Zappella, and R. Vidal. “Surgical Gesture Classification from Video Data”. In: *Medical Image Computing and Computer-Assisted Intervention ? MICCAI 2012*. Ed. by N. Ayache, H. Delingette, P. Golland, and K. Mori. Lecture Notes in Computer Science 7510. Springer Berlin Heidelberg, Jan. 1, 2012, pp. 34–41. ISBN: 978-3-642-33414-6 978-3-642-33415-3.
- [Kla08] U. Klank, N. Padoy, H. Feussner, and N. Navab. “Automatic Feature Generation in Endoscopic Images”. In: *International Journal of Computer Assisted Radiology and Surgery* 3.3-4 (Sept. 1, 2008), pp. 331–339. ISSN: 1861-6410, 1861-6429. DOI: 10.1007/s11548-008-0223-8.
- [Lal13] F. Lalys, D. Bouget, L. Riffaud, and P. Jannin. “Automatic Knowledge-Based Recognition of Low-Level Tasks in Ophthalmological Procedures”. In: *International Journal of Computer Assisted Radiology and Surgery* 8.1 (Jan. 1, 2013), pp. 39–49. ISSN: 1861-6410, 1861-6429. DOI: 10.1007/s11548-012-0685-6.
- [Lal11] F. Lalys, L. Riffaud, D. Bouget, and P. Jannin. “An Application-Dependent Framework for the Recognition of High-Level Surgical Tasks in the OR”. In: *Medical Image Computing and Computer-Assisted Intervention ? MICCAI 2011*. Ed. by G. Fichtinger, A. Martel, and T. Peters. Lecture Notes in Computer Science 6891. Springer Berlin Heidelberg, Jan. 1, 2011, pp. 331–338. ISBN: 978-3-642-23622-8 978-3-642-23623-5.
- [BAH17] A. Bux, P. Angelov, and Z. Habib. “Vision Based Human Activity Recognition: A Review”. In: *Advances in Computational Intelligence Systems* (2017), pp. 341–371. DOI: 10.1007/978-3-319-46562-3_23.
- [Kha13] W. Khan. “Image Segmentation Techniques: A Survey”. In: *Journal of Image and Graphics* 1.4 (2013), pp. 166–170.
- [App09] J. Appenrodt, A. Al-Hamadi, M. Elmezain, and B. Michaelis. “Data Gathering for Gesture Recognition Systems Based on Mono Color-, Stereo Color- and Thermal Cameras”. In: *Future Generation Information Technology*. Ed. by Y.-h. Lee, T.-h. Kim, W.-c. Fang, and D. ?zak. Lecture Notes in Computer Science. Berlin, Heidelberg: Springer, 2009, pp. 78–86. ISBN: 978-3-642-10509-8. DOI: 10.1007/978-3-642-10509-8_10.
- [MVC09] N. Memarian, A. N. Venetsanopoulos, and T. Chau. “Infrared Thermography as an Access Pathway for Individuals with Severe Motor Impairments”. In: *Journal of NeuroEngineering and Rehabilitation* 6.1 (Apr. 16, 2009), p. 11. ISSN: 1743-0003. DOI: 10.1186/1743-0003-6-11.

- [Ste73] J. Steketee. "Spectral Emissivity of Skin and Pericardium". In: *Physics in Medicine and Biology* 18.5 (1973), p. 686. ISSN: 0031-9155. DOI: 10.1088/0031-9155/18/5/307.
- [Tog89] T. Togawa. "Non-Contact Skin Emissivity: Measurement from Reflectance Using Step Change in Ambient Radiation Temperature". In: *Clinical Physics and Physiological Measurement* 10.1 (Feb. 1989), pp. 39–48. ISSN: 0143-0815. DOI: 10.1088/0143-0815/10/1/004.
- [Rog12] A. Rogalski. "History of Infrared Detectors". In: *Opto-Electronics Review* 20.3 (Sept. 1, 2012), pp. 279–308. ISSN: 1896-3757. DOI: 10.2478/s11772-012-0037-7.
- [Kru01] P. W. Kruse. *Uncooled Thermal Imaging Arrays, Systems and Applications*. Tutorial Texts in Optical Engineering 51. Bellingham, Wash: SPIE Press, 2001. 89 pp. ISBN: 978-0-8194-4122-5.
- [SJC58] R. Smith, F. Jones, and R. Chasmar. *The Detection and Measurement of Infrared Radiation*. Oxford: Clarendon, 1958.
- [SSZ09] N. Salvaggio, L. D. Stroebel, and R. D. Zakia. *Basic Photographic Materials and Processes*. 3rd ed. Amsterdam ; Boston: Focal Press/Elsevier, 2009. 462 pp. ISBN: 978-0-240-80984-7.
- [Sol12] S. Soldan. "On Extended Depth of Field to Improve the Quality of Automated Thermographic Measurements in Unknown Environments". In: *Quantitative InfraRed Thermography Journal*. 9.2. 2012, pp. 135–150.
- [Lah12] B. B. Lahiri, S. Bagavathiappan, T. Jayakumar, and J. Philip. "Medical Applications of Infrared Thermography: A Review". In: *Infrared Physics & Technology* 55.4 (July 2012), pp. 221–235. ISSN: 1350-4495. DOI: 10.1016/j.infrared.2012.03.007.
- [Cha15] K. Chang et al. "Rapid vs. Delayed Infrared Responses after Ischemia Reveal Recruitment of Different Vascular Beds". In: *Quantitative InfraRed Thermography Journal* 12.2 (July 3, 2015), pp. 173–183. ISSN: 1768-6733. DOI: 10.1080/17686733.2015.1046677.
- [RA12] E. F. J. Ring and K. Ammer. "Infrared Thermal Imaging in Medicine". In: *Physiological Measurement* 33.3 (2012), R33. ISSN: 0967-3334. DOI: 10.1088/0967-3334/33/3/R33.

-
- [HP11] C. Herman and M. Pirtini Cetingul. “Quantitative Visualization and Detection of Skin Cancer Using Dynamic Thermal Imaging”. In: *Journal of Visualized Experiments* (May 5, 2011). ISSN: 1940-087X. DOI: 10.3791/2679.
- [Den10] A. E. Denoble, N. Hall, C. F. Pieper, and V. B. Kraus. “Patellar Skin Surface Temperature by Thermography Reflects Knee Osteoarthritis Severity”. In: *Clinical Medicine Insights: Arthritis and Musculoskeletal Disorders* 3 (Jan. 1, 2010), CMAMD.S5916. ISSN: 1179-5441. DOI: 10.4137/CMAMD.S5916.
- [Pol17] G. Polidori, Y. Renard, S. Lorimier, H. Pron, S. Derruau, and R. Taiar. “Medical Infrared Thermography Assistance in the Surgical Treatment of Axillary Hidradenitis Suppurativa: A Case Report”. In: *International Journal of Surgery Case Reports* 34 (Jan. 1, 2017), pp. 56–59. ISSN: 2210-2612, 2210-2612. DOI: 10.1016/j.ijscr.2017.03.015. pmid: 28359047.
- [Bag09] S. Bagavathiappan, T. Saravanan, J. Philip, T. Jayakumar, B. Raj, R. Karunanithi, T. M. R. Panicker, M. P. Korath, and K. Jagadeesan. “Infrared Thermal Imaging for Detection of Peripheral Vascular Disorders”. In: *Journal of Medical Physics / Association of Medical Physicists of India* 34.1 (2009), pp. 43–47. ISSN: 0971-6203. DOI: 10.4103/0971-6203.48720. pmid: 20126565.
- [LEP17] P. H. Lin, A. Echeverria, and M. J. Poi. “Infrared Thermography in the Diagnosis and Management of Vasculitis”. In: *Journal of Vascular Surgery Cases and Innovative Techniques* 3.3 (Sept. 1, 2017), pp. 112–114. ISSN: 2468-4287. DOI: 10.1016/j.jvscit.2016.12.002.
- [BRB79] H. A. Bird, E. F. Ring, and P. A. Bacon. “A Thermographic and Clinical Comparison of Three Intra-Articular Steroid Preparations in Rheumatoid Arthritis.” In: *Annals of the Rheumatic Diseases* 38.1 (Feb. 1, 1979), pp. 36–39. ISSN: 0003-4967, 1468-2060. DOI: 10.1136/ard.38.1.36. pmid: 373651.
- [Ess78] W. Esselinckx, P. A. Bacon, E. F. Ring, D. Crooke, A. J. Collins, and D. Demottaz. “A Thermographic Assessment of Three Intra-Articular Prednisolone Analogues given in Rheumatoid Synovitis.” In: *British Journal of Clinical Pharmacology* 5.5 (1978), pp. 447–451. ISSN: 1365-2125. DOI: 10.1111/j.1365-2125.1978.tb01653.x.
- [Spa08] S. J. Spalding, C. K. Kwoh, R. Boudreau, J. Enama, J. Lunich, D. Huber, L. Denes, and R. Hirsch. “Three-Dimensional and Thermal Surface Imaging Produces Reliable Measures of Joint Shape and Temperature: A Potential Tool for

- Quantifying Arthritis”. In: *Arthritis Research & Therapy* 10.1 (2008), R10. ISSN: 1478-6354. DOI: 10.1186/ar2360.
- [Ger14] E. Gerasimova, B. Audit, S. G. Roux, A. Khalil, O. Gileva, F. Argoul, O. Naimark, and A. Arneodo. “Wavelet-Based Multifractal Analysis of Dynamic Infrared Thermograms to Assist in Early Breast Cancer Diagnosis”. In: *Frontiers in Physiology* 5 (May 8, 2014). ISSN: 1664-042X. DOI: 10.3389/fphys.2014.00176.
- [Omr16] R. Omranipour et al. “Comparison of the Accuracy of Thermography and Mammography in the Detection of Breast Cancer”. In: *Breast Care* 11.4 (2016), pp. 260–264. ISSN: 1661-3791, 1661-3805. DOI: 10.1159/000448347. pmid: 27721713.
- [Vre13] T. D. Vreugdenburg, C. D. Willis, L. Mundy, and J. E. Hiller. “A Systematic Review of Elastography, Electrical Impedance Scanning, and Digital Infrared Thermography for Breast Cancer Screening and Diagnosis”. In: *Breast Cancer Research and Treatment* 137.3 (Feb. 1, 2013), pp. 665–676. ISSN: 0167-6806, 1573-7217. DOI: 10.1007/s10549-012-2393-x.
- [Tan08] X. Tang, H. Ding, Y.-e. Yuan, and Q. Wang. “Morphological Measurement of Localized Temperature Increase Amplitudes in Breast Infrared Thermograms and Its Clinical Application”. In: *Biomedical Signal Processing and Control* 3.4 (Oct. 1, 2008), pp. 312–318. ISSN: 1746-8094. DOI: 10.1016/j.bspc.2008.04.001.
- [Ger16] E. Gerasimova-Chechkina et al. “Comparative Multifractal Analysis of Dynamic Infrared Thermograms and X-Ray Mammograms Enlightens Changes in the Environment of Malignant Tumors”. In: *Frontiers in Physiology* 7 (2016). ISSN: 1664-042X. DOI: 10.3389/fphys.2016.00336.
- [Fio18] W. C. Fiorotti, E. d. R. Constantino, L. de Lima, A. Conci, R. A. Fernandes, R. T. M. Leal, J. A. Landeiro, and M. A. Acioly. “Intraoperative Infrared Thermography for the Functional Imaging and Tumor Resection Maximization of a Low-Grade Glioma: Technical Case Report”. In: *Arquivos Brasileiros de Neurocirurgia: Brazilian Neurosurgery*. XXXII Congresso Brasileiro de Neurocirurgia. Vol. 37. Thieme Revinter Publicações Ltda, Sept. 2018, A1011. DOI: 10.1055/s-0038-1672847.
- [Nay17] E. Naydenov, K. Minkin, M. Penkov, S. Nachev, and W. Stummer. “Infrared Thermography in Surgery of Newly Diagnosed Glioblastoma Multiforme: A Technical Case Report”. In: *Case Reports in Oncology* 10.1 (Apr. 18, 2017), pp. 350–355. ISSN: 1662-6575. DOI: 10.1159/000470832.

-
- [Gor04] A. M. Gorbach, J. D. Heiss, L. Kopylev, and E. H. Oldfield. “Intraoperative Infrared Imaging of Brain Tumors”. In: *Journal of Neurosurgery* 101.6 (Dec. 2004), pp. 960–969. ISSN: 0022-3085. DOI: 10.3171/jns.2004.101.6.0960.
- [Jus15] M. Just, C. Chalopin, M. Unger, D. Halama, T. Neumuth, A. Dietz, and M. Fischer. “Monitoring of Microvascular Free Flaps Following Oropharyngeal Reconstruction Using Infrared Thermography: First Clinical Experiences”. In: *European Archives of Oto-Rhino-Laryngology* (Sept. 18, 2015), pp. 1–9. ISSN: 0937-4477, 1434-4726. DOI: 10.1007/s00405-015-3780-9.
- [Rat18] P. Rathmann, C. Chalopin, D. Halama, P. Giri, J. Meixensberger, and D. Lindner. “Dynamic Infrared Thermography (DIRT) for Assessment of Skin Blood Perfusion in Cranioplasty: A Proof of Concept for Qualitative Comparison with the Standard Indocyanine Green Video Angiography (ICGA)”. In: *International Journal of Computer Assisted Radiology and Surgery* 13.3 (Mar. 1, 2018), pp. 479–490. ISSN: 1861-6429. DOI: 10.1007/s11548-017-1683-5.
- [dWWM12a] L. de Weerd, S. Weum, and J. B. Mercer. “Dynamic Infrared Thermography (DIRT) in the Preoperative, Intraoperative and Postoperative Phase of DIEP Flap Surgery”. In: *Journal of Plastic, Reconstructive & Aesthetic Surgery* 65.5 (May 2012), pp. 694–695. ISSN: 17486815. DOI: 10.1016/j.bjps.2011.11.013.
- [Bha07] B. Bhatia, T. Oates, Y. Xiao, and P. Hu. “Real-Time Identification of Operating Room State from Video”. In: *AAAI*. Vol. 2. 2007, pp. 1761–1766.
- [SF15] N. Schuster and J. Franks. “Depth of Field in Modern Thermal Imaging”. In: *SPIE Defense+ Security*. International Society for Optics and Photonics. Ed. by G. C. Holst and K. A. Krapels. May 12, 2015, 94520J-94520J-11. DOI: 10.1117/12.2086937.
- [PH11] M. Pirtini Çetingül and C. Herman. “Quantification of the Thermal Signature of a Melanoma Lesion”. In: *International Journal of Thermal Sciences* 50.4 (Apr. 1, 2011), pp. 421–431. ISSN: 1290-0729. DOI: 10.1016/j.ijthermalsci.2010.10.019.
- [WW10] C.-H. Wong and F.-C. Wei. “Microsurgical Free Flap in Head and Neck Reconstruction”. In: *Head & Neck* 32.9 (Sept. 1, 2010), pp. 1236–1245. ISSN: 1097-0347. DOI: 10.1002/hed.21284.
- [dWWM12b] L. de Weerd, S. Weum, and J. B. Mercer. “Dynamic Infrared Thermography: A Useful Tool in the Preoperative Planning of Deep Inferior Epigastric Perforator

-
- Flaps”. In: *Annals of Plastic Surgery* 68.6 (June 2012), pp. 639–640. ISSN: 0148-7043. DOI: 10.1097/SAP.0b013e318244413a.
- [Köh19] H. Köhler et al. “Evaluation of Hyperspectral Imaging (HSI) for the Measurement of Ischemic Conditioning Effects of the Gastric Conduit during Esophagectomy”. In: *Surgical Endoscopy* 33.11 (Nov. 1, 2019), pp. 3775–3782. ISSN: 1432-2218. DOI: 10.1007/s00464-019-06675-4.
- [Jan19] B. Jansen-Winkel et al. “Determination of the Transection Margin during Colorectal Resection with Hyperspectral Imaging (HSI)”. In: *International Journal of Colorectal Disease* 34.4 (Apr. 1, 2019), pp. 731–739. ISSN: 1432-1262. DOI: 10.1007/s00384-019-03250-0.
- [Goe20] E. Goetze, D. G. E. Thiem, M. W. Gielisch, and P. W. Kämmerer. “Identification of Cutaneous Perforators for Microvascular Surgery Using Hyperspectral Technique ? A Feasibility Study on the Antero-Lateral Thigh”. In: *Journal of Cranio-Maxillofacial Surgery* 48.11 (Nov. 1, 2020), pp. 1066–1073. ISSN: 1010-5182. DOI: 10.1016/j.jcms.2020.09.005.
- [Nis21] S. P. Nischwitz, H. Luze, M. Schellnegger, S. J. Gatterer, A.-C. Tuca, R. Winter, and L.-P. Kamolz. “Thermal, Hyperspectral and Laser Doppler Imaging: Non-Invasive Tools for Detection of the Deep Inferior Epigastric Artery Perforators? A Prospective Comparison Study”. In: *Journal of Personalized Medicine* 11.10 (10 Oct. 2021), p. 1005. DOI: 10.3390/jpm11101005.

Darstellung des eigenen Beitrags

Die veröffentlichten Artikel wurden während meiner Tätigkeiten als wissenschaftlicher Mitarbeiter am Innovation Center Computer Assisted Surgery der medizinischen Fakultät der Universität Leipzig unter Betreuung von Herrn Prof. Thomas Neumuth angefertigt.

In dem Artikel *Automatic Recognition of Surgical Activities* wurden chirurgische Gesten mittels einer Thermographiekamera aufgezeichnet und ausgewertet. Die Studiendurchführung, die Aufbereitung und Auswertung der erhobenen Daten erfolgte durch mich persönlich.

In dem Artikel *Automatic depth scanning system for 3D infrared thermography* wurde ein System für die Rekonstruktion eines Bildes, das über alle Tiefenebenen scharf ist, entwickelt und evaluiert. Die Implementierung der Software erfolgte durch Herrn Adrian Franke. Die Studiendurchführung, die Auswertung und Darstellung der Ergebnisse erfolgte durch mich persönlich.

In dem Artikel *Automatic detection of perforator vessels using infrared thermography in reconstructive surgery* wurden die Positionen möglicher Perforatorgefäße durch Untersuchung der Temperaturverteilung auf der Hautoberfläche extrahiert. Die in der Probandenstudie thermographischen Aufnahmen wurden durch Frau Miriam Markfurt aufgenommen. Die Annotation der Thermogramme erfolgte durch Herrn Dr. Dirk Halama und Frau Miriam Markfurt. Die Implementierung des Detektionsalgorithmus, die Nachverarbeitung der Daten sowie die Auswertung und Darstellung der Ergebnisse erfolgte durch mich persönlich.

In den gemeinsam verfassten Artikeln hatte ich als Erstautor einen wesentlichen Anteil.

Leipzig, den 1. April 2022

Prof. Thomas Neumuth

Name

Unterschrift

Dr. Claire Chalopin

Name

Unterschrift

Dr. Dirk Halama

Name

Unterschrift

Michael Unger

Name

Unterschrift

Erklärung über die eigenständige Abfassung der Arbeit

Hiermit erkläre ich, dass ich die vorliegende Arbeit selbstständig und ohne unzulässige Hilfe oder Benutzung anderer als der angegebenen Hilfsmittel angefertigt habe. Ich versichere, dass Dritte von mir weder unmittelbar noch mittelbar eine Vergütung oder geldwerte Leistungen für Arbeiten erhalten haben, die im Zusammenhang mit dem Inhalt der vorgelegten Dissertation stehen, und dass die vorgelegte Arbeit weder im Inland noch im Ausland in gleicher oder ähnlicher Form einer anderen Prüfungsbehörde zum Zweck einer Promotion oder eines anderen Prüfungsverfahrens vorgelegt wurde. Alles aus anderen Quellen und von anderen Personen übernommene Material, das in der Arbeit verwendet wurde oder auf das direkt Bezug genommen wird, wurde als solches kenntlich gemacht. Insbesondere wurden alle Personen genannt, die direkt an der Entstehung der vorliegenden Arbeit beteiligt waren. Die aktuellen gesetzlichen Vorgaben in Bezug auf die Zulassung der klinischen Studien, die Bestimmungen des Tierschutzgesetzes, die Bestimmungen des Gentechnikgesetzes und die allgemeinen Datenschutzbestimmungen wurden eingehalten. Ich versichere, dass ich die Regelungen der Satzung der Universität Leipzig zur Sicherung guter wissenschaftlicher Praxis kenne und eingehalten habe.

1. April 2022

Datum

Unterschrift

Liste der Veröffentlichungen

Journalartikel (peer-reviewed)

M. Unger, C. Chalopin, and T. Neumuth, “Vision-based online recognition of surgical activities”, *International Journal of Computer Assisted Radiology and Surgery*, vol. 9, no. 6, pp. 979–986, Mar. 25, 2014, ISSN: 1861-6410, 1861-6429. DOI: 10.1007/s11548-014-0994-z.

M. Unger, A. Franke, and C. Chalopin, “Automatic depth scanning system for 3D infrared thermography”, *Current Directions in Biomedical Engineering*, vol. 2, no. 1, pp. 369–372, 2016. DOI: 10.1515/cdbme-2016-0162.

M. Unger, D. Black, N. M. Fischer, T. Neumuth, and B. Glaser, “Design and evaluation of an eye tracking support system for the scrub nurse”, *The International Journal of Medical Robotics and Computer Assisted Surgery*, vol. 0, e1954, ja Aug. 22, 2018, ISSN: 1478-596X. DOI: 10.1002/rcs.1954.

M. Unger, M. Markfort, D. Halama, and C. Chalopin, “Automatic detection of perforator vessels using infrared thermography in reconstructive surgery”, *International Journal of Computer Assisted Radiology and Surgery*, vol. 14, no. 3, pp. 501–507, Mar. 1, 2019, ISSN: 1861-6429. DOI: 10.1007/s11548-018-1892-6.

M. Unger, J. Berger, B. Gerold, and A. Melzer, “Robot-assisted Ultrasound-guided Tracking of Anatomical Structures for the Application of Focused Ultrasound”, *Current Directions in Biomedical Engineering*, vol. 6, no. 3, pp. 123–126, Sep. 1, 2020. DOI: 10.1515/cdbme-2020-3032.

M. Unger, J. Berger, and A. Melzer, “Robot-Assisted Image-Guided Interventions”, *Frontiers in Robotics and AI*, vol. 0, 2021, ISSN: 2296-9144. DOI: 10.3389/frobt.2021.664622.

Journalartikel, Ko-Autor (peer-reviewed)

M. Just, C. Chalopin, M. Unger, D. Halama, T. Neumuth, A. Dietz, and M. Fischer, “Monitoring of microvascular free flaps following oropharyngeal reconstruction using infrared thermography: First clinical experiences”, *European Archives of Oto-Rhino-Laryngology*, pp. 1–9, Sep. 18, 2015, ISSN: 0937-4477, 1434-4726. DOI: 10.1007/s00405-015-3780-9.

D. Black, M. Unger, N. Fischer, R. Kikinis, H. Hahn, T. Neumuth, and B. Glaser, “Auditory display as feedback for a novel eye-tracking system for sterile operating room interaction”, *International Journal of Computer Assisted Radiology and Surgery*, pp. 1–9, Oct. 27, 2017, ISSN: 1861-6410, 1861-6429. DOI: 10.1007/s11548-017-1677-3.

J. Berger, M. Unger, L. Landgraf, R. Bieck, T. Neumuth, and A. Melzer, “Assessment of Natural User Interactions for Robot-Assisted Interventions”, *Current Directions in Biomedical Engineering*, vol. 4, no. 1, pp. 165–168, Sep. 1, 2018, ISSN: 2364-5504. DOI: 10.1515/cdbme-2018-0041.

- J. Berger, M. Unger, L. Landgraf, and A. Melzer, “Evaluation of an IEEE 11073 SDC Connection of two KUKA Robots towards the Application of Focused Ultrasound in Radiation Therapy”, *Current Directions in Biomedical Engineering*, vol. 5, no. 1, pp. 149–152, Sep. 1, 2019. DOI: 10.1515/cdbme-2019-0038.
- S. Hu, X. Zhang, M. Unger, I. Patties, A. Melzer, and L. Landgraf, “Focused Ultrasound-Induced Cavitation Sensitizes Cancer Cells to Radiation Therapy and Hyperthermia”, *Cells*, vol. 9, no. 12, p. 2595, 12 Dec. 2020. DOI: 10.3390/cells9122595.
- C. M. Reich, M. Unger, L. Melzer, T. Jochimsen, B. Sattler, O. Sabri, and A. Melzer, “Developing an Intuitive and Feasible Setup for In-room Control During MRI-guided Interventions”, *Current Directions in Biomedical Engineering*, vol. 6, no. 3, pp. 280–283, Sep. 1, 2020, ISSN: 2364-5504. DOI: 10.1515/cdbme-2020-3071.
- C. M. Reich, B. Sattler, T. H. Jochimsen, M. Unger, L. Melzer, L. Landgraf, H. Barthel, O. Sabri, and A. Melzer, “Practical setting and potential applications of interventions guided by PET/MRI”, *The quarterly journal of nuclear medicine and molecular imaging*, vol. 65, no. 1, pp. 43–50, Mar. 2021, ISSN: 1824-4785. DOI: 10.23736/s1824-4785.20.03293-8.
- X. Zhang, M. Bobeica, M. Unger, A. Bednarz, B. Gerold, I. Patties, A. Melzer, and L. Landgraf, “Focused ultrasound radiosensitizes human cancer cells by enhancement of DNA damage”, *Strahlentherapie und Onkologie*, Apr. 22, 2021, ISSN: 1439-099X. DOI: 10.1007/s00066-021-01774-5.
- X. Zhang, L. Landgraf, N. Bailis, M. Unger, T. H. Jochimsen, and A. Melzer, “Image-Guided High-Intensity Focused Ultrasound, A Novel Application for Interventional Nuclear Medicine?”, *Journal of Nuclear Medicine*, vol. 62, no. 9, pp. 1181–1188, Sep. 1, 2021, ISSN: 0161-5505, 2159-662X. DOI: 10.2967/jnumed.120.256230.

Konferenzartikel

- M. Unger, C. Chalopin, and T. Neumuth, “Automatic gesture recognition based on thermography”, in *47th Annual Conference of the German Society for Biomedical Engineering (BMT)*, Sep. 7, 2013.
- M. Unger *et al.*, “Concept for integrating a MR-compatible robotic arm into the clinical infrastructure”, presented at the EUFUS 2017, Leipzig, Germany, Oct. 2017.
- M. Unger, J. Berger, L. Landgraf, and A. Melzer, “Robotic Positioning for Image-Guided Ultrasound Interventions”, in *CURAC Tagungsband*, Reutlingen, Aug. 2019, pp. 16–17, ISBN: 978-3-00-063717-9.
- M. Unger, J. Berger, B. Gerold, and A. Melzer, “Robot-assisted Ultrasound-guided Tracking of Anatomical Structures for the Application of Focused Ultrasound”, presented at the 54th Annual Conference of the German Society for Biomedical Engineering (BMT), Leipzig, Germany, 2020.
- M. Unger, J. Berger, B. Gerold, and A. Melzer, “Robot-assisted Ultrasound-guided Tracking of Anatomical Structures for the Application of Focused Ultrasound”, presented at the 32nd Annual SMIT Congress, 2020.

Konferenzartikel, Ko-Autor

J. Berger, M. Unger, L. Landgraf, T. Neumuth, and A. Melzer, “Towards integration of robotics for focused ultrasound (FUS) surgery and radiation therapy into the clinical treatment process”, in *26th International EAES Congress*, London, UK, 30.05.-01.06.2018.

B. Glaser, M. Unger, T. Schellenberg, and T. Neumuth, “Use Cases für sterile blickgesteuerte Mensch-Maschine-Interaktionskonzepte im digitalen Operationssaal”, in *14. Jahrestagung Der Gesellschaft Für Computer- Und Roboterassistierte Chirurgie e. V. - CURAC*, Bremen, Sep. 17, 2015.

J. Berger, M. Unger, T. Jochimse, B. Satter, U. Roy, L. Landgraf, T. Neumuth, O. Sabri, and A. Melzer, “A. Concepts for robot-assisted focused ultrasound to support radiation therapy”, presented at the 6th International Symposium on Focused Ultrasound, Reston, USA, 2018.

J. Berger, M. Unger, T. Jochimse, B. Sattler, L. Landgraf, O. Sabri, and A. Melzer, “Approaches to support radiation therapy by robot-assisted focused ultrasound”, presented at the Society for Medical Innovation and Technology (SMIT), Seoul, Korea, 2018.

J. Berger, M. Unger, T. Jochimsen, B. Sattler, U. Roy, L. Landgraf, T. Neumuth, O. Sabri, and A. Melzer, “Concepts for robot-assisted focused ultrasound to support radiation therapy”, in *FUS Foundation Symposium*, Reston Virginia, USA, 2018.

J. Berger, M. Unger, J. Keller, R. Bieck, L. Landgraf, T. Neumuth, and A. Melzer, “Assessment of Natural User Interactions for Robot-Assisted Interventions”, presented at the BMT (Aachen), 2018.

J. Berger, M. Unger, J. Keller, R. Bieck, L. Landgraf, T. Neumuth, and A. Melzer, “Kollaborative Interaktion für die roboterassistierte ultraschallgeführte Biopsie”, in *CURAC Tagungsband*, 2018.

J. Berger, M. Unger, J. Keller, R. Bieck, L. Landgraf, T. Neumuth, and A. Melzer, “Natural User Interaction for Collaborative Robot-Assisted Needle Targeting”, presented at the The 12th Hamlyn Symposium on Medical Robotics, 2018.

J. Berger, M. Unger, L. Landgraf, X. Zhang, S. Hu, D. McLeod, T. Neumuth Thomas, and A. Melzer, “Towards integrating robotics for combined focused ultrasound and radiation therapy into the treatment process”, presented at the 18th Annual International Symposium for Therapeutic Ultrasound (ISTU), Nashville, USA, 2018.

L. Landgraf *et al.*, “Combination of focused ultrasound hyperthermia (FUS-HT) and radiation therapy: Validation of in vitro effects in a preliminary study”, presented at the 52nd Annual Conference of the German Society for Biomedical Engineering (BMT) (Aachen), 2018.

X. Zhang, L. Landgraf, M. Unger, U. Roy, I. Patties, D. McLeod, and A. Melzer, “Focused ultrasound-induced hyperthermia and radiation therapy for combined treatment of brain and prostate cancer cells in vitro”, presented at the Society for Medical Innovation and Technology (SMIT), Seoul, Korea, 2018.

X. Zhang, L. Landgraf, M. Unger, U. Roy, I. Patties, D. McLeod, T. Neumuth, and A. Melzer, “Focused ultrasound-hyperthermia and radiation therapy for combined treatment of brain and prostate tumors ? preliminary studies in vitro”, in *FUS Foundation Symposium*, Reston Virginia, USA, 2018.